M.S. Thesis
04/14/2020
1100 hrs. (CT)

Thermal modeling of additive manufacturing using graph theory: Validation with directed energy deposition

Jordan Severson
Advisors
Dr. Prahalada Rao & Dr. Kevin Cole
Department of Mechanical and Materials Engineering
University of Nebraska-Lincoln

Acknowledgements

Thesis committee for valuable inputs and guidance.

- Dr. Prahalada Rao
- Dr. Kevin Cole
- Dr. Jeff Shield

Acknowledgements

National Science Foundation for funding this work through

CMMI 1752069 CAREER (PI: Dr. Prahalada Rao)

Acknowledgements

The data for this work was requested from the publication at Pennsylvania State University (PSU)

J. C. Heigel, P. Michaleris, and E. W. Reutzel, "Thermo-mechanical model development and validation of directed energy deposition additive manufacturing of Ti–6Al–4V," Additive Manufacturing, vol. 5, pp. 9-19, 1/1/2015 2015.

Outline

- Introduction
- Methodology
- Results
- Conclusions

Outline

- Introduction
  - Background
  - Goal and Motivation
  - Current Efforts (Literature)
- Methodology
- Results
- Conclusions

Background

Directed energy deposition (DED) is an additive manufacturing (AM) process.

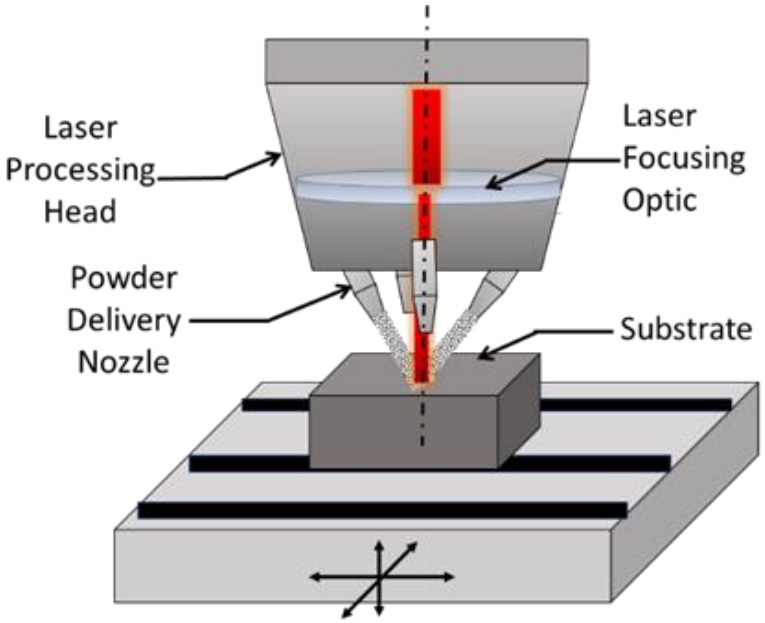

Why use directed energy deposition?

AGT 1500 (M1 Abrams Engine)

- Cost savings of over $5M per year
- Added convenience for short interval maintenance

Source: Tom Cobbs, Product Manager at Optomec®

URL: https://optomec.com/how-3d-metal-printing-saves-time-and-lowers-costs-ded-for-repair-of-industrial-components/

Why use directed energy deposition?

1. Produce complex geometries (e.g., satellites & spacecraft)
2. Repair rather than replace

Broken gear teeth

After repair with DED

After machining

Inconel Helical Gear Repair

- Lead time reduction: 8 weeks to 1 day
- Enhanced material properties

Source: Tom Cobbs, Product Manager at Optomec®

URL: https://optomec.com/how-3d-metal-printing-saves-time-and-lowers-costs-ded-for-repair-of-industrial-components

Defects in AM occur at multiple scales.

The thermal aspects of the process affect the quality of the part.

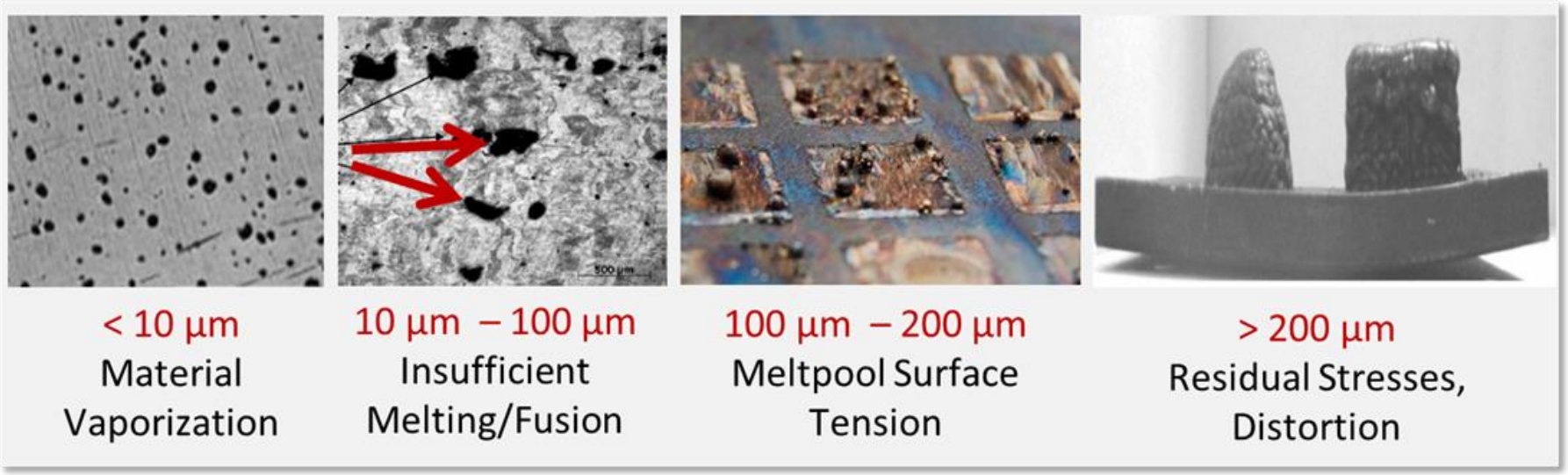

W. J. Sames, F. List, S. Pannala, R. R. Dehoff, and S. S. Babu, "The Metallurgy and Processing Science of Metal Additive Manufacturing," International Materials Reviews, vol. 61, pp. 315-360, 2016.

Thermal Aspects of DED

Certain heat transfer-related assumptions made in the context of the laser powder bed fusion (LPBF) must be relaxed for the DED process.

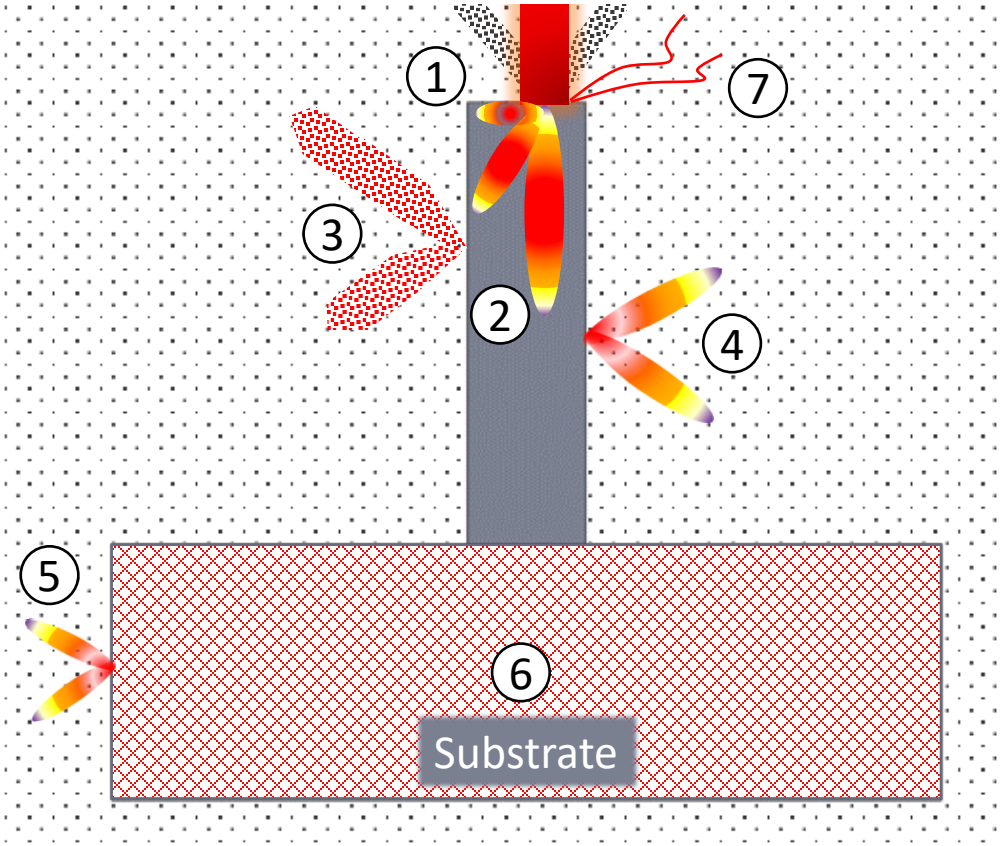

Salient Thermal Phenomena in DED.

1. *Part-Energy Source Interaction Zone*
   Latent Heat of Melting & Solidification.
   Meltpool Marangoni Convection
2. *Part-Part Interaction Zone*
   Conductive Heat Transfer
3. *Part-Gas Interaction Zone*
   Radiative Heat Transfer
4. *Part-Gas Interaction Zone*
   Forced Convective Heat Transfer
5. *Substrate-Gas Interaction Zone*
   Free Convective Heat Transfer
6. *Substrate-Clamp Interaction Zone*
   Conduction
7. *Laser-Part-Gas Interaction Zone*
   Reflection, Absorption, Keyhole melting-effect

To mitigate severity of defects, the fundamental link between process parameters, thermal phenomena, and part properties must be understood.

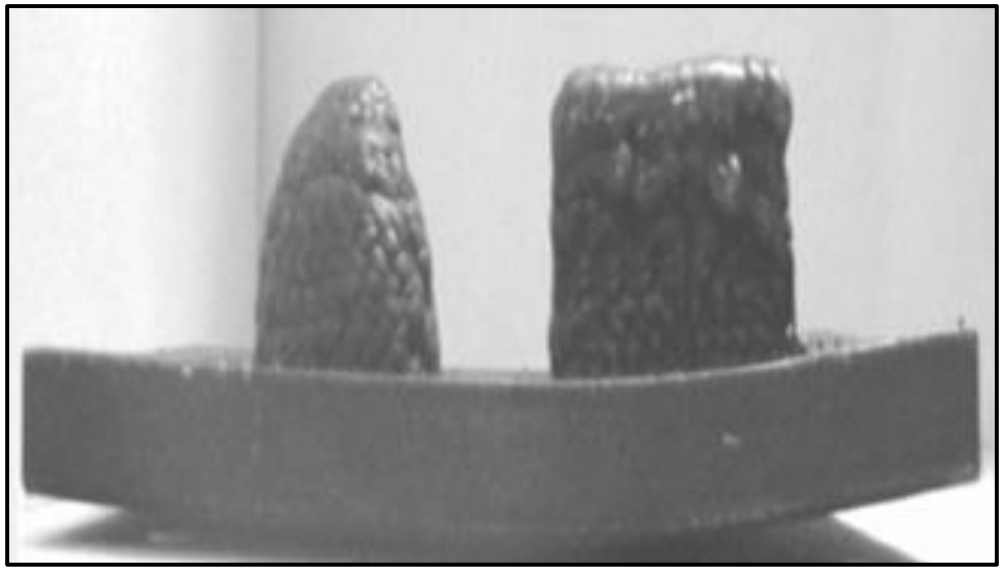

Goal and Motivation

Graph theory approach for thermal modeling has been validated and published in the context of the LPBF process.

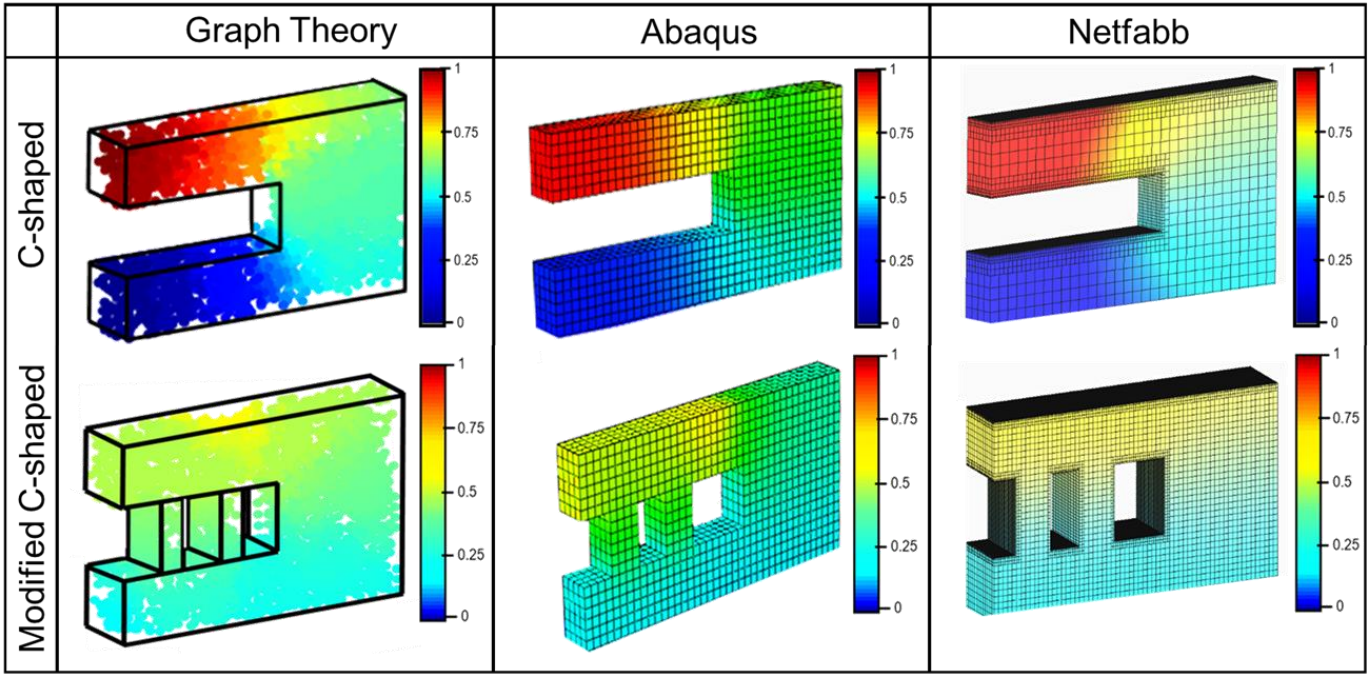

Error (SMAPE)	Total number of nodes	Graph theory approach time	FE analysis time
16%	1,000	0.5 min	200 min (2,000 elements)
10%	5,000	18 min	
8%	8,000	41 min	

K. Cole, R. Yavari, P.Rao, *Computational heat transfer with spectral graph theory: Quantitative verification,* International Journal of Thermal Sciences, Volume 153, July 2020, (Accepted, in-press, available online). doi: 10.1016/j.ijthermalsci.2020.106383

Goal

Validate the graph theory approach for thermal modeling for the DED process

Simulation (Literature)

Some, but not all, weld modeling principles fit well in the DED framework.

Transferrable Weld Modeling Principles?

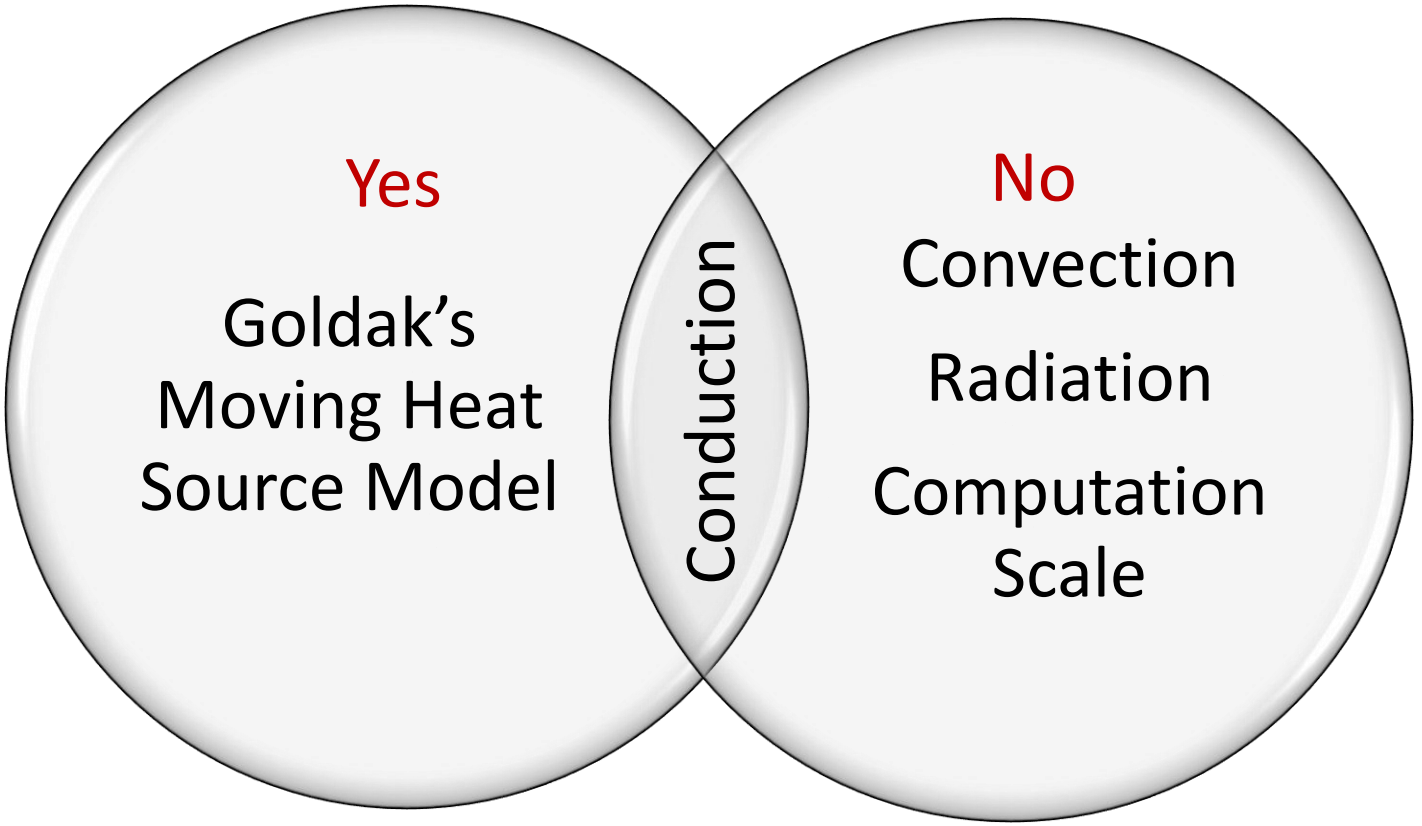

Simulation (Literature)

Differences between welding and DED are demonstrated by considering the temperature of the base material and number of passes.

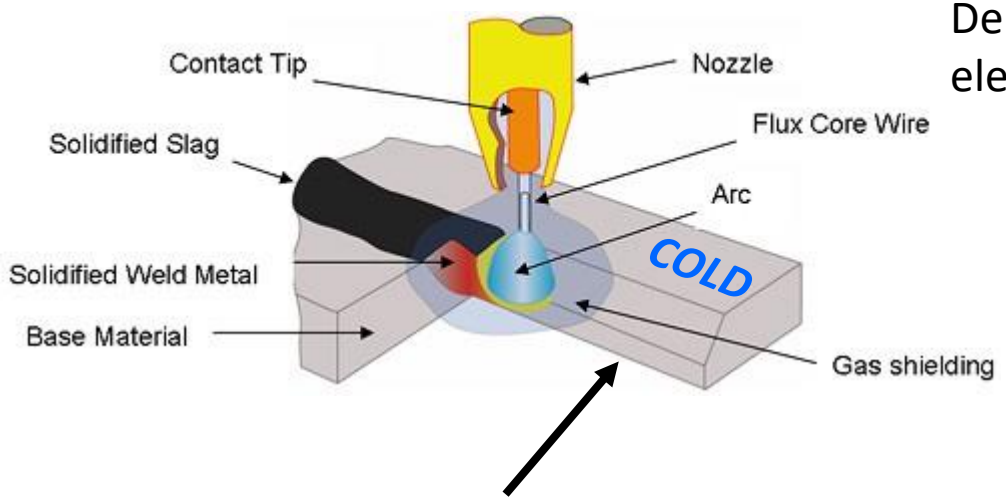

Prefabricated metal at ambient temperature

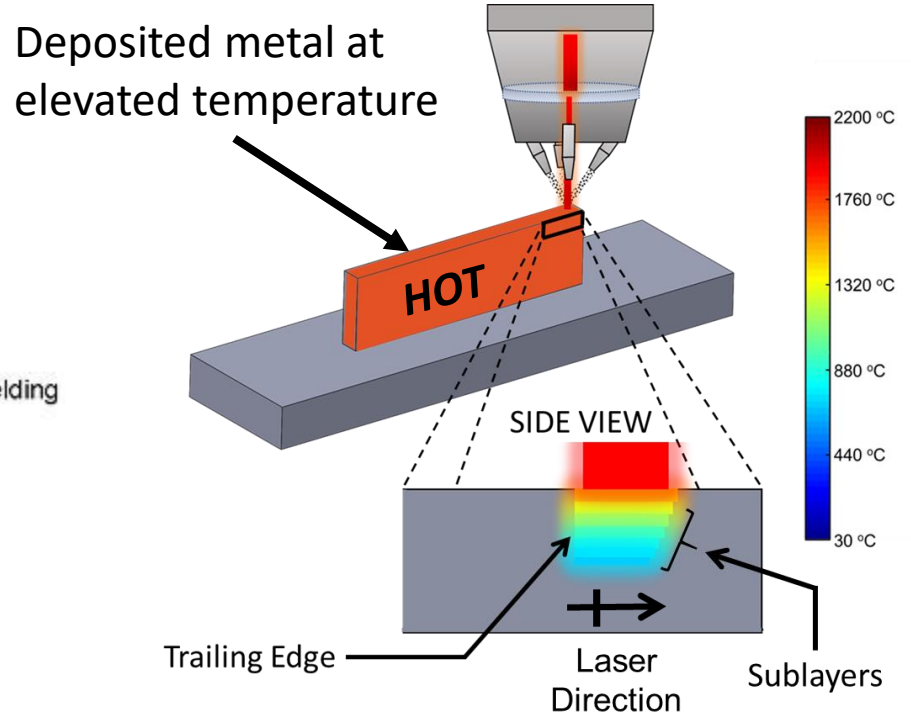

Number of passes: 1

Number of passes: 62

Source: metalsupplies.com

Convection (Literature)

Researchers have assumed one of the following:

1. Convective heat loss is negligible (from weld modeling)
2. Uniformly distributed free convection loss
3. Uniformly distributed forced convection loss
4. Complex convection models (developed empirically or from CFD model)
5. Measurement-based convection models (Jarred Heigel)
6. Combination of free and forced convection (graph theory)

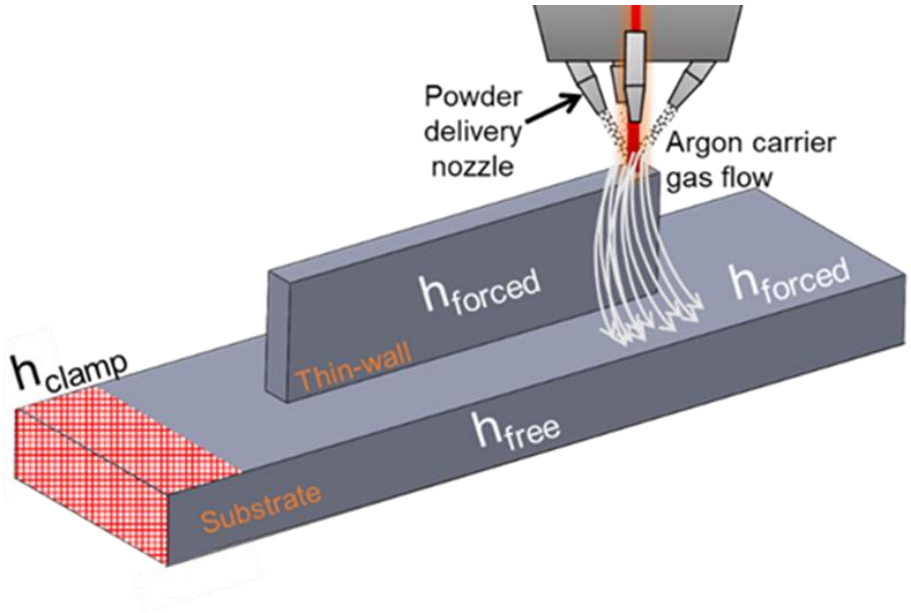

Computation Techniques (Literature)

To increase computational efficiency, Michaleris proposed and tested two material deposition methods:

1. *Quiet Elements:* assigns scaled material properties to elements that have not been deposited
2. *Inactive Elements:* not included in analysis until they are deposited

Quiet Elements

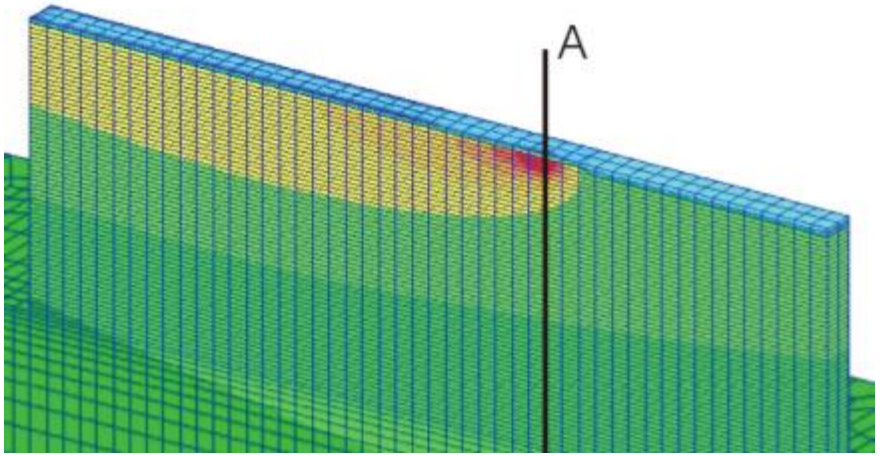

Inactive Elements

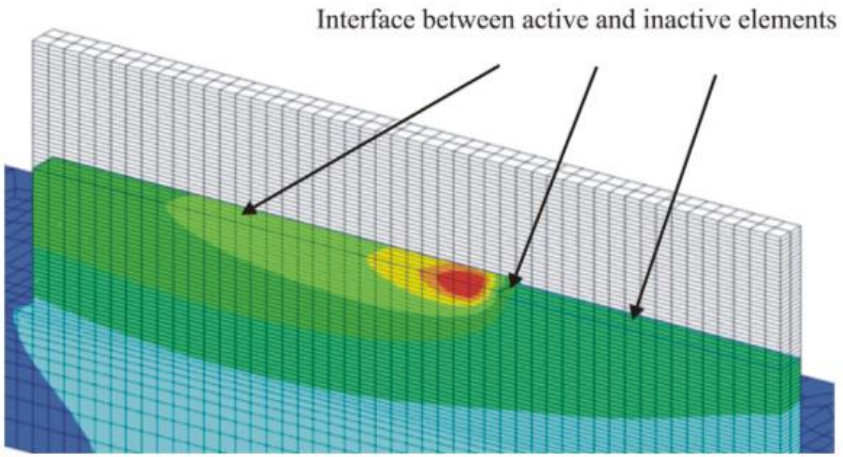

P. Michaleris, "Modeling metal deposition in heat transfer analyses of additive manufacturing processes," *Finite Elements in Analysis and Design,* vol. 86, pp. 51-60, 4/28/2014 2014.

Outline

- Context
- Methodology
  - Experiments
  - Simulation Procedure
    - → Graph Theory
    - → Implementation
  - Goldak's Double Ellipsoid Model
- Results
- Conclusions

Experimental Builds

Three Ti-6Al-4V single-track thin walls were deposited on separate clamped substrates of equal dimensions.

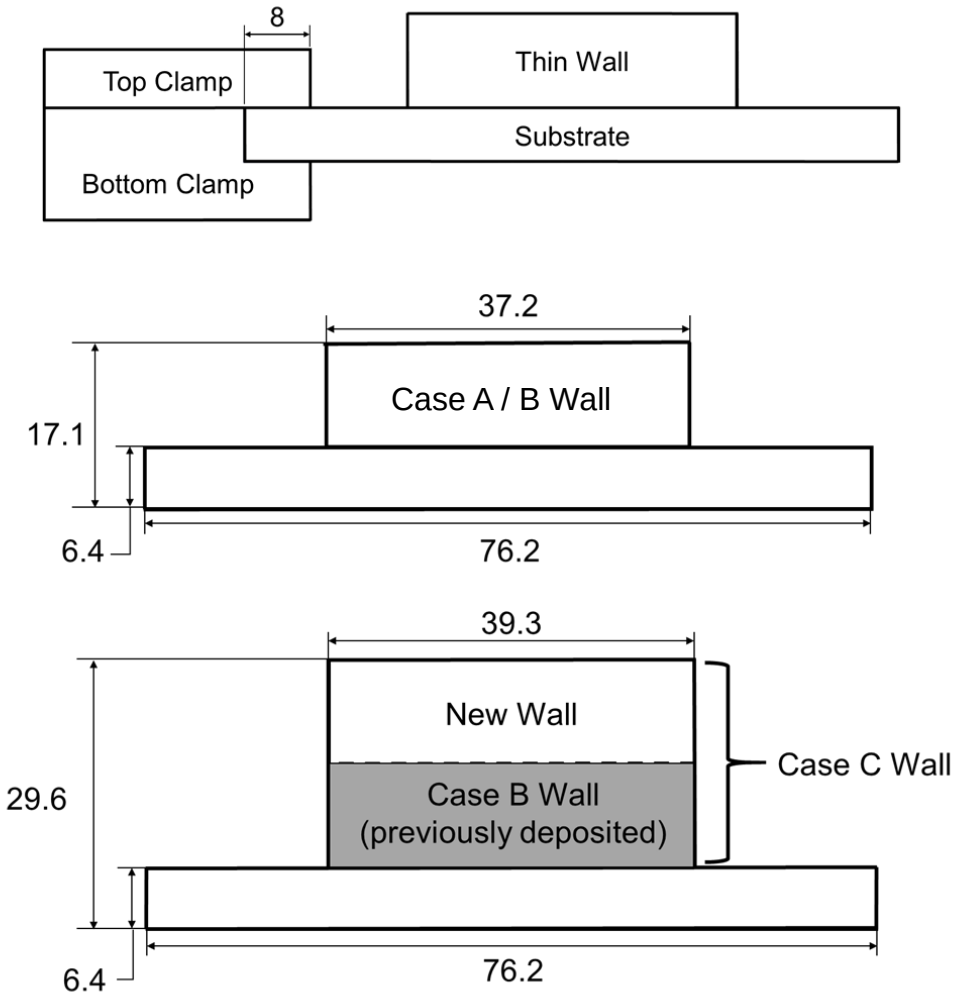

Experimental Builds

- Each substrate was clamped at one end
- A thermocouple collected thermal history at a specified location in the substrate
- Aluminum tape was used to shield TC 2 from forced convection loss in the first case

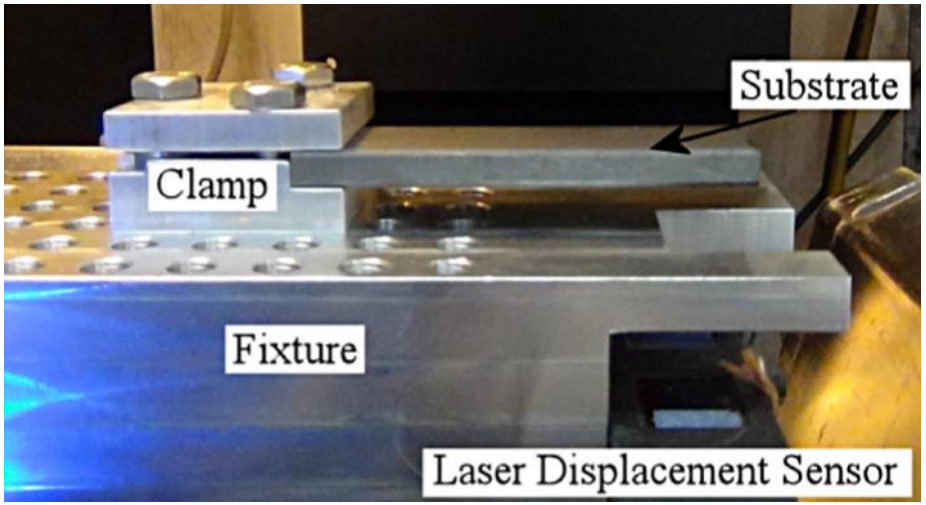

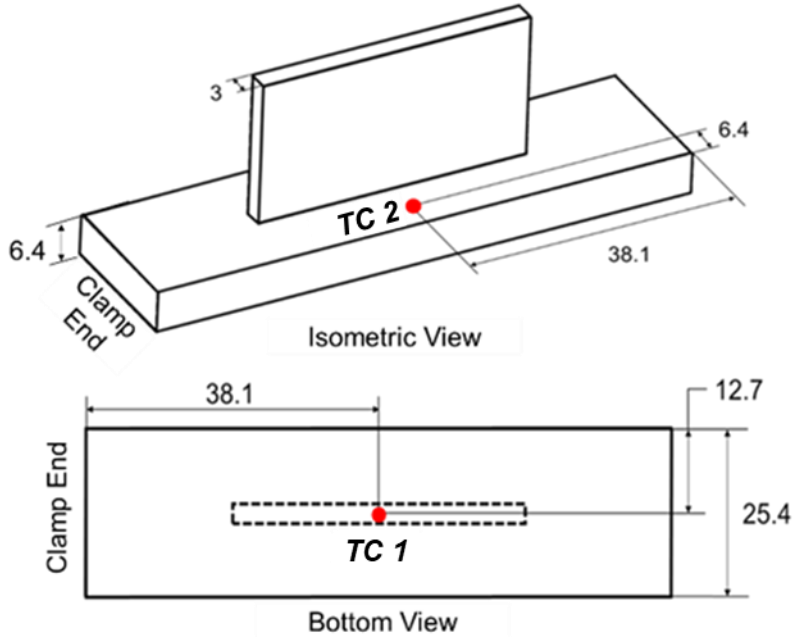

J. C. Heigel, P. Michaleris, and E. W. Reutzel, "Thermo-mechanical model development and validation of directed energy deposition additive manufacturing of Ti–6Al–4V," Additive Manufacturing, vol. 5, pp. 9-19, 1/1/2015 2015.

Summary of Experiments

Temperature excursions are more prevalent with increased dwell time.

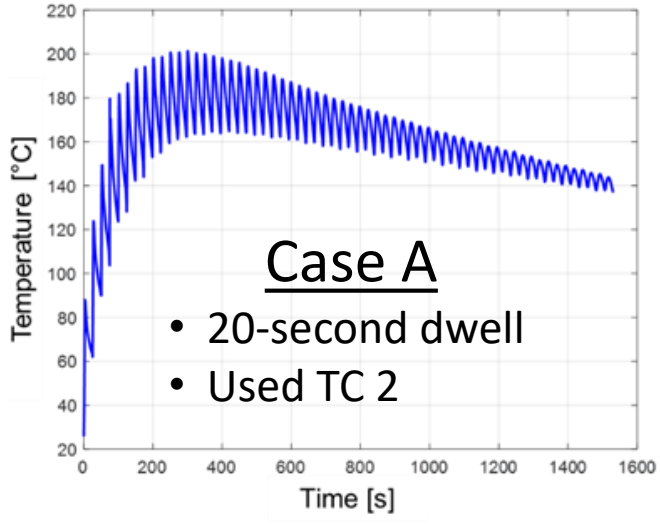

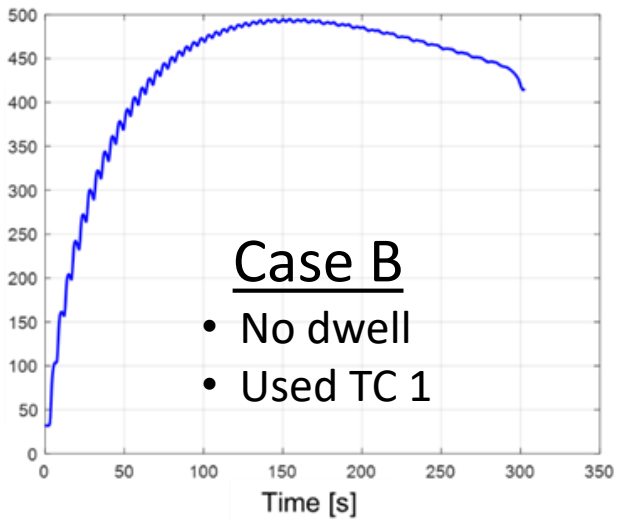

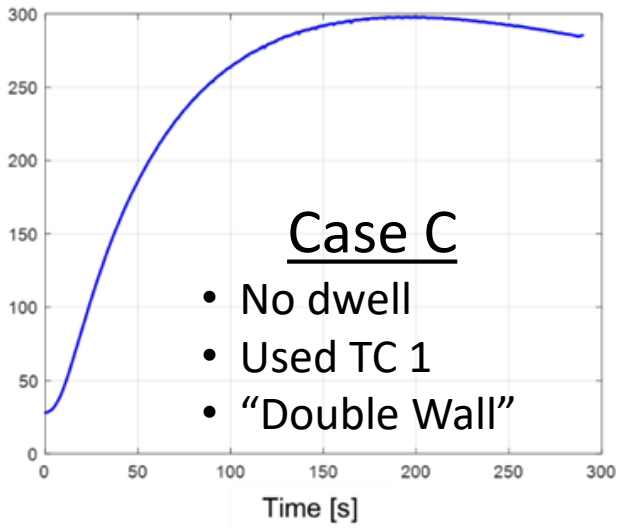

Case	A	B	C
Measured Laser Power [W]	415	410	415
Travel Speed [mm·s^{-1}]		8.5	
Powder delivery rate [g·min^{-1}]		3.0	
Additional dwell time [s]	20	0	0
Wall height [mm]	10.7	11.2	23.2
Measured wall length [mm]	37.2	39.2	39.3
Measured wall width [mm]	2.2	3.0	3.1
Measured Layer thickness [mm]	0.1726	0.1806	0.1871
Laser spot size [mm]		1.5	
Standoff Distance [mm]		11.4	

Graph Theory

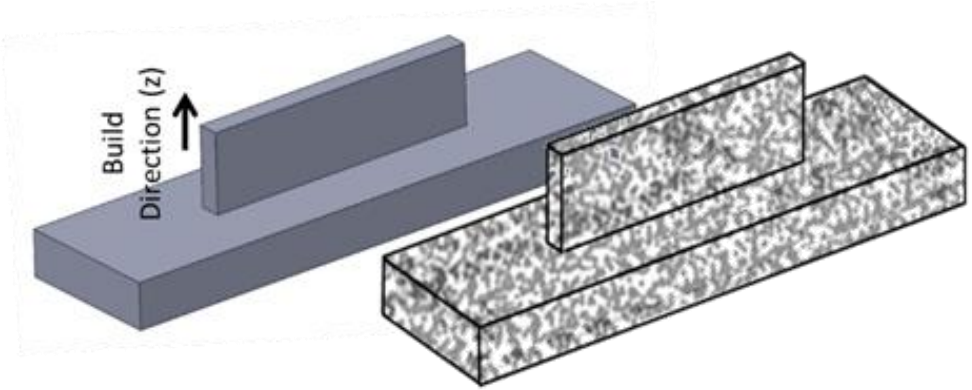

Step 1- Convert the part into a set of discrete nodes

M. R. Yavari, K. Cole, and P. Rao, "Thermal Modeling in Metal Additive Manufacturing using Graph Theory," *ASME Transactions, Journal of Manufacturing Science and Engineering,* vol. 141, pp. 071007-27, July 2019.

Graph Theory

Step 1: Discretizing the part geometry into nodes and blocks

- Convert part into discrete nodes
- Number of nodes is set at a certain number per unit volume (called node density)
- Part is then divided into layers, hatches, and blocks

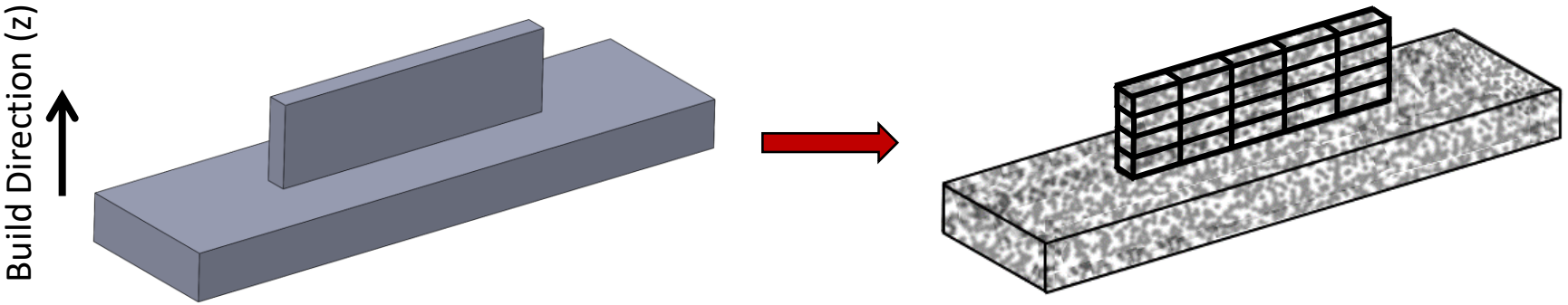

Graph Theory

Step 2: Constructing a network graph from the cloud of discrete nodes

- Each node is connected to its nearest neighboring nodes
- Nearness is defined by ε (called the neighborhood distance)
- Matrix formed by placing a_{ij} in a row *i* and column *j* is called the adjacency matrix, $\mathbf{A} = [a_{ij}]$

$$a_{ij} = \begin{cases} e^{-(c_i - c_j)^2/\sigma^2} & if (c_i - c_j)^2 \leq \varepsilon \\ 0 & otherwise \end{cases}$$

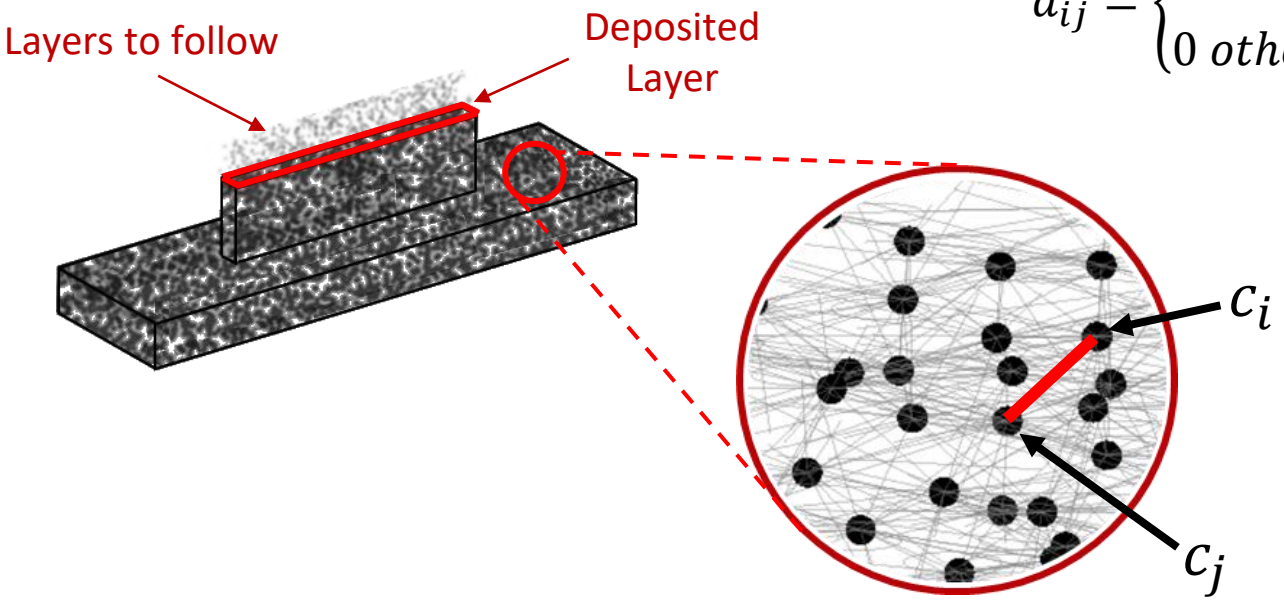

Graph Theory

Step 3(a): Heat loss through conduction

- Sole heat transfer mechanism between nodes is conduction
- A time step involves heating of nodes inside a block, one block at a time (t_b = 0.922 s)

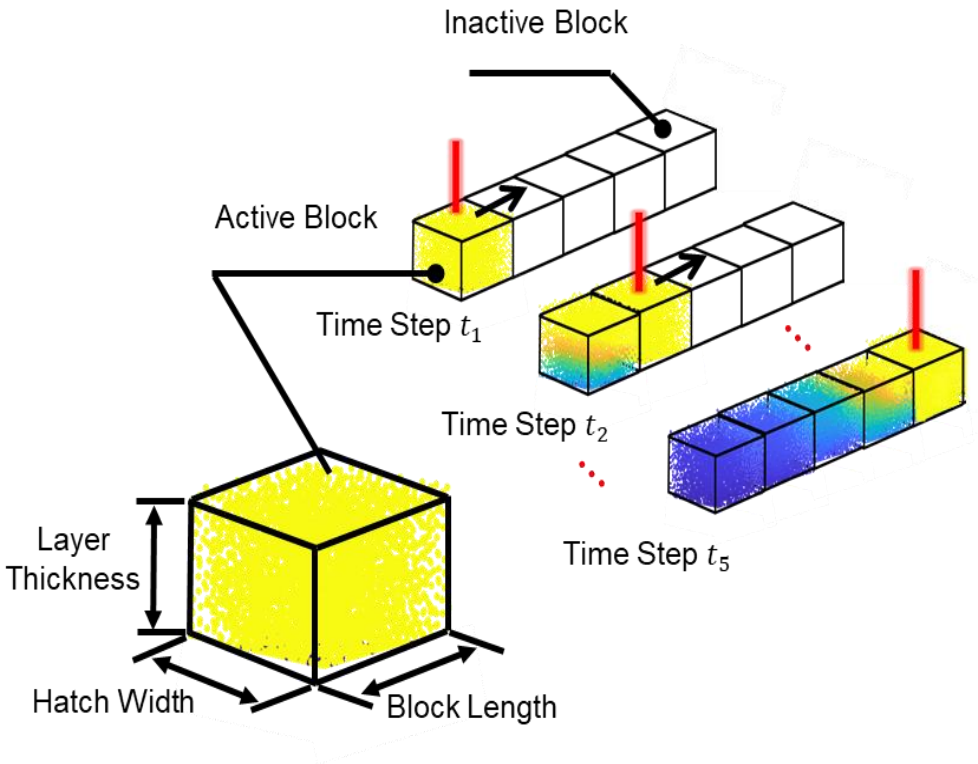

$$\mathbf{T}_c = \boldsymbol{\Phi} e^{-\alpha g \boldsymbol{\Lambda} t_b} \boldsymbol{\Phi}' \mathrm{T}_0$$

Variable	Definition
$\mathbf{T}_c$	Temp. vector at time t (end of time step)
$\boldsymbol{\Phi}$	Laplacian Eigenvector matrix
α	Thermal diffusivity of Ti-6Al-4V
g	Gain factor
$\boldsymbol{\Lambda}$	Laplacian Eigenvalue matrix
t_b	Time step (= 0.922 s)
T_0	Temp. vector at time 0

Graph Theory

Step 3(b): Heat loss through convection

- Heat loss through convection from the nodes on the surface of the part occurs in tandem with conduction

From Step 3(a): $\mathbf{T}_c = \boldsymbol{\phi} e^{-\alpha g \boldsymbol{\Lambda} t_b} \boldsymbol{\phi}' \mathrm{T}_0$

$$\mathbf{T}_b = \mathbf{T}_c e^{-\beta t_b}$$

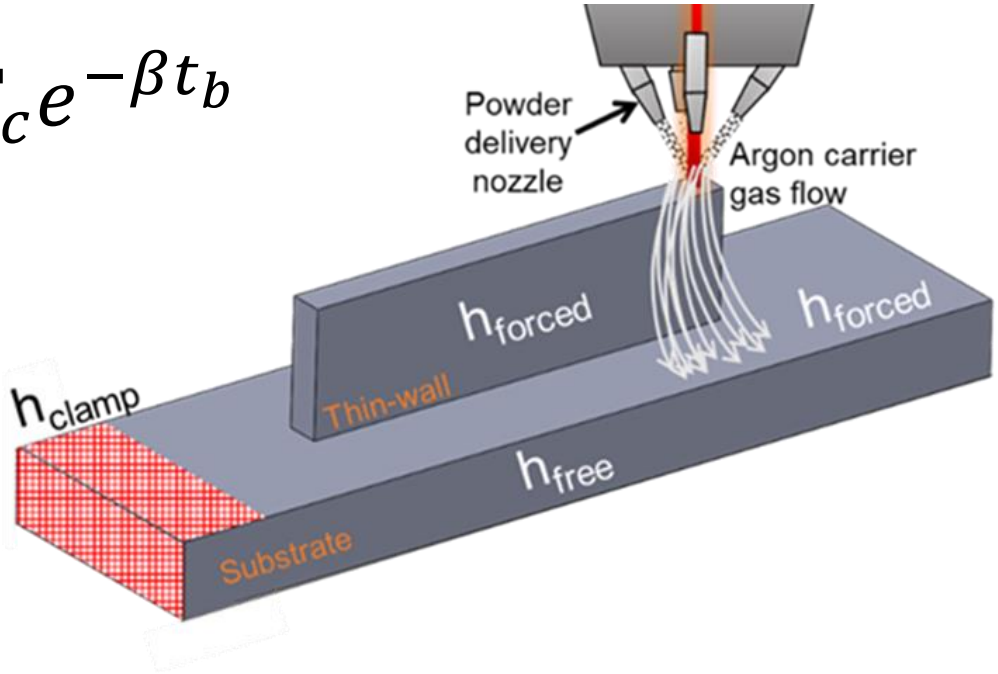

Graph Theory

Step 3(b): Heat loss through convection

- β is the inverse time constant can be related to the heat transfer coefficient

$$\mathbf{T}_b = \mathbf{T}_c e^{-\beta t_b}$$

$$\beta = \frac{h}{\rho \times L \times C_p}$$

Variable	Definition	Units
β	Inverse time constant	s^{-1}
h	Heat Transfer Coefficient	$W \cdot m^{-2} \cdot K^{-1}$
ρ	Density of Ti-6Al-4V	$kg \cdot m^{-3}$
L	Block Length	m
C_p	Specific Heat	$J \cdot kg^{-1} \cdot K^{-1}$

Graph Theory

Step 3(c): Obtaining temperature at the end of a layer (after dwell)

- Heat is allowed to dissipate
- Identical to Steps 3(a) and (b), except iterative for a period equal to the dwell time (t_d)

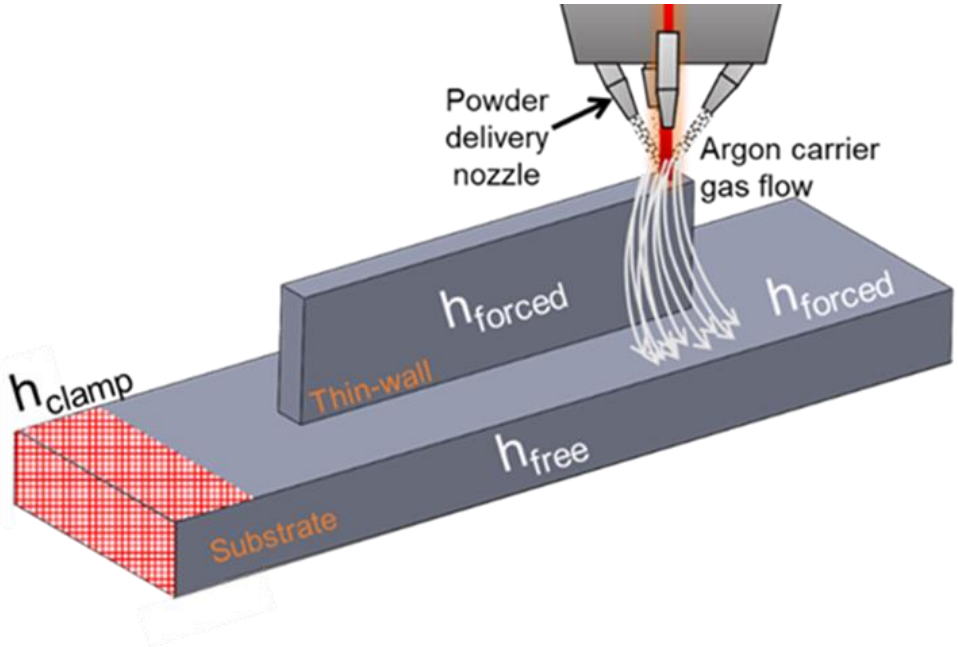

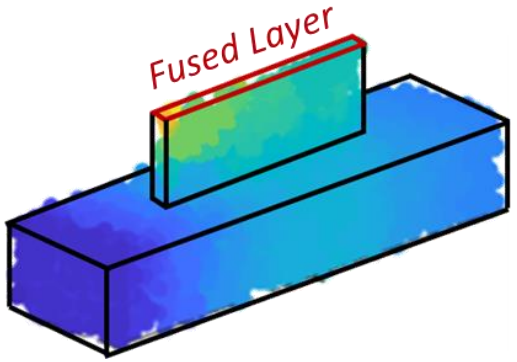

$$\mathbf{T}_{Lc} = \boldsymbol{\Phi} e^{-\alpha g \boldsymbol{\Lambda} t_d} \boldsymbol{\Phi}' \mathbf{T}_b$$

$$\mathbf{T}_{Lf} = \mathbf{T}_{Lc} e^{-\beta t_d}$$

- t_d = 20 s for Case A
- t_d = 3 s for Case B and Case C

Graph Theory

Step 4: Recording nodal temperatures in vector

- Steps 3(a), (b), and (c) are looped until the last layer is built
- The temperature of each node at each time step is recorded in a vector **T** (thermal history vector)

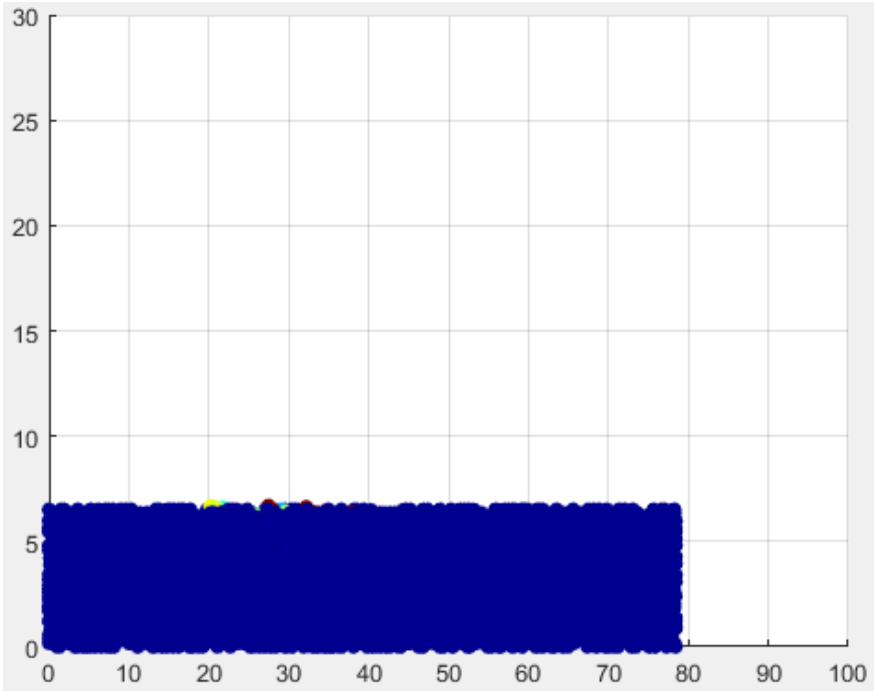

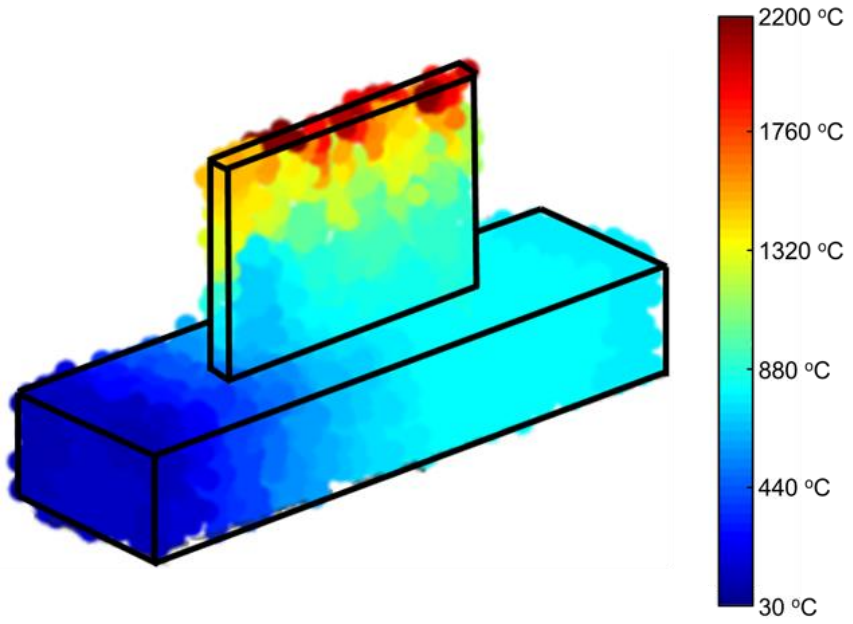

Implementation

- Case A was used to calibrate the graph theory approach
  - Chosen because of the prominent temperature cycles
  - Combination of ε and g resulting in the lowest Mean Absolute Percentage Error (MAPE) was selected

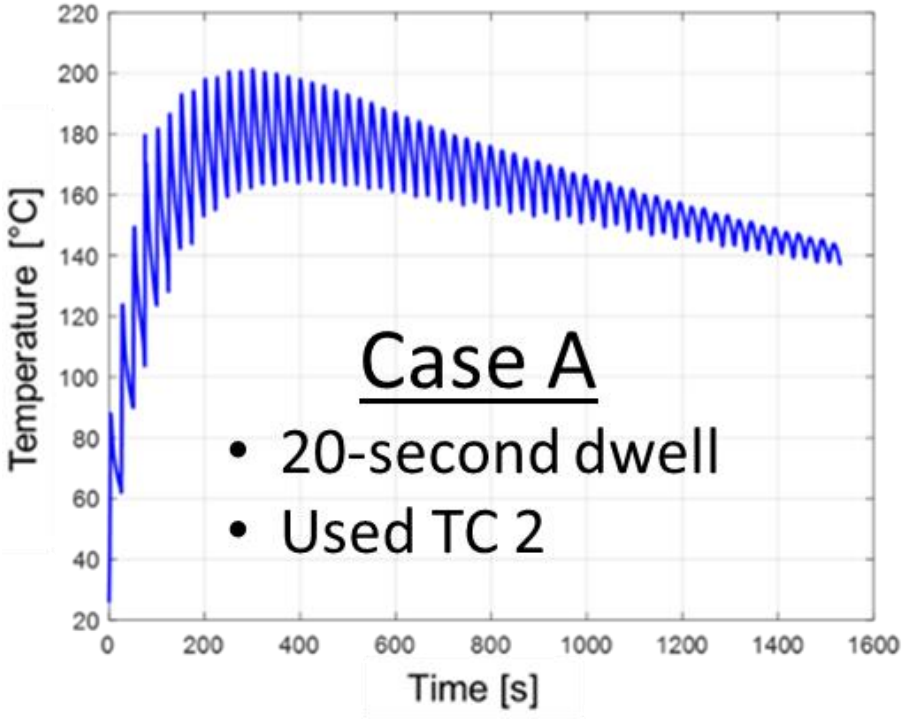

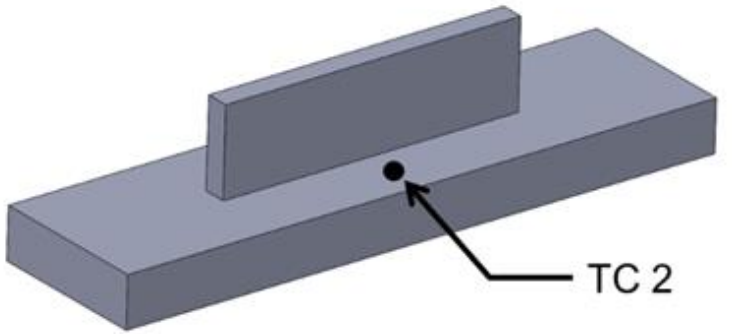

Calibration

Implementation

Calibration was conducted at three node densities and three meltpool temperatures.

Nodes per Block	Total Number of Nodes	Number of Nodes in Wall	Node Density (nodes/mm^3)	Neighborhood Size, ε (mm)	Gain Factor (g)		
					T_0 = 1900 ^oC (mm^{-2})	T_0 = 2200 ^oC (mm^{-2})	T_0 = 2450 ^oC (mm^{-2})
1	2830	310	0.2355	4.5	8	10	12
2	5660	620	0.4709	4.75	1	1.5	1.95
3	8490	930	0.7064	5.5	0.12	0.15	0.17

Calibration

Implementation

Heat transfer coefficients are estimated in the calibration step and are held constant throughout all simulation cases.

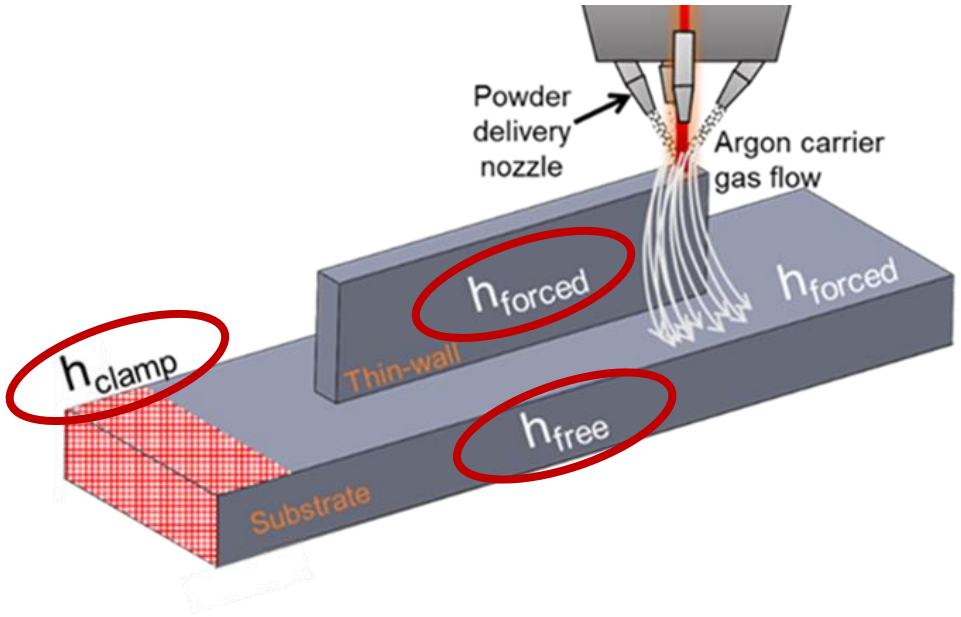

$$\beta = \frac{h}{\rho \times L \times C_p}$$

Implementation

Free convection was estimated first by observing the prediction during the initial rising action of the experiment.

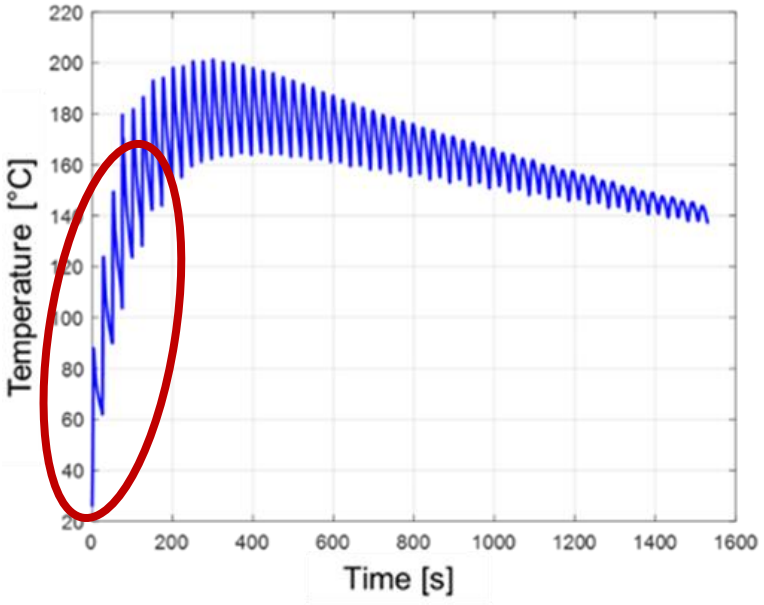

$$\beta = \frac{h}{\rho \times L \times C_p}$$

Heat Transfer Coefficient	Inverse Time Constant in Graph-theoretic Method [s^{-1}]	Equivalent Heat Transfer Coefficient [$W \cdot m^{-2} \cdot K^{-1}$]
Clamp	0.05 (200× free)	981.2
Forced	0.0025 (10× free)	49.1
Free	0.00027	5.3

How do these compare with Heigel?

Estimated heat transfer coefficients were compared to Heigel's measurement-based convection model.

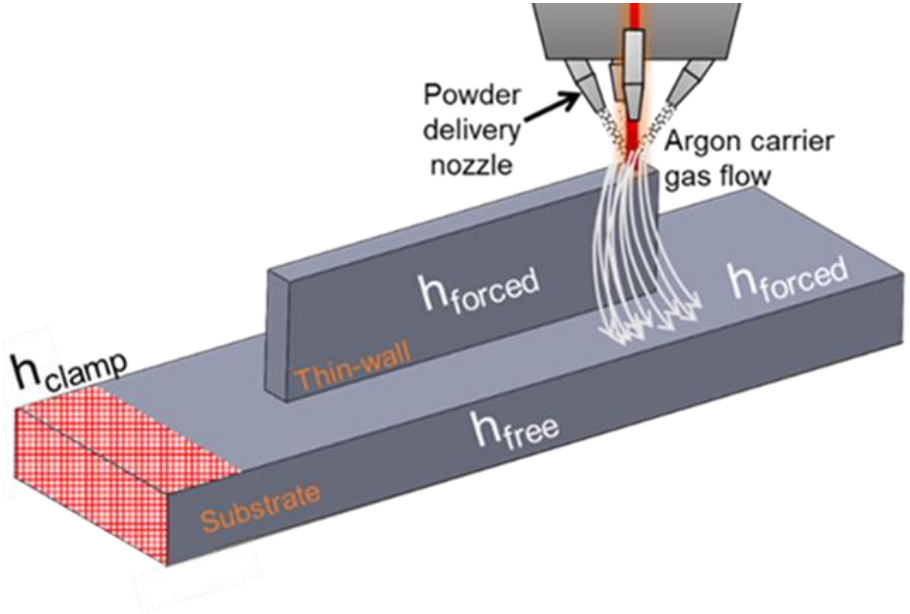

$$\beta = \frac{h}{\rho \times L \times C_p}$$

Heat Transfer Coefficient	Inverse Time Constant in Graph-theoretic Method [s^{-1}]	Equivalent Heat Transfer Coefficient [$W \cdot m^{-2} \cdot K^{-1}$]	Heigel's Model [$W \cdot m^{-2} \cdot K^{-1}$]
Clamp	0.05	981.2	N/A
Forced	0.0025	49.1	25-60
Free	0.00027	5.3	10

Implementation

- The Cartesian coordinates of one node, called the sensor node, are defined with the coordinates of the thermocouple
- How do we account for aluminum tape used to shield the thermocouple from forced convection?
  - Sensor node is “buried” at a depth of 0.1 mm below the surface of the substrate

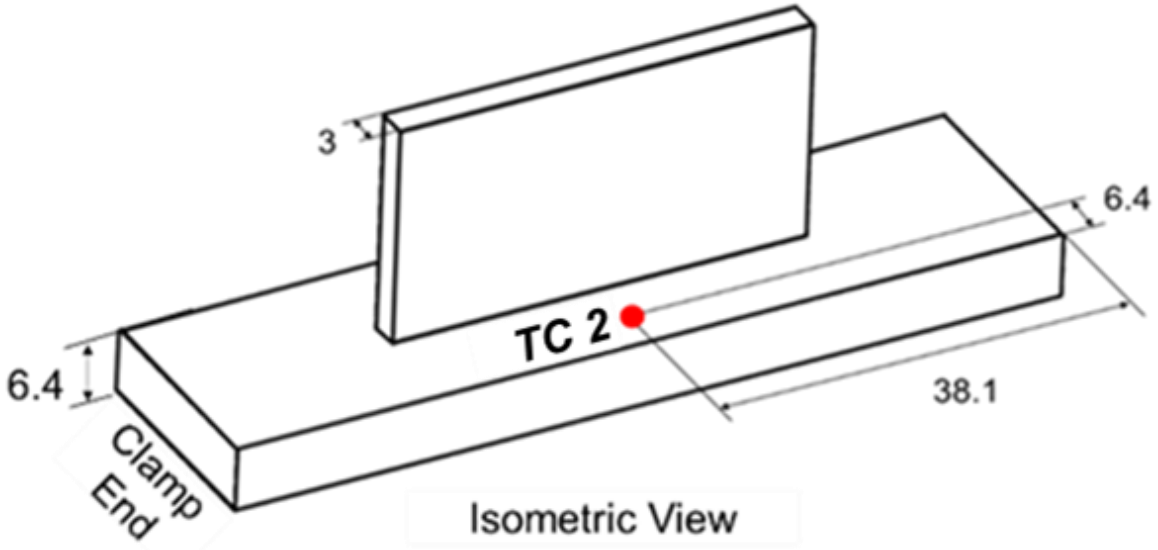

Sensor Location

Implementation

- Material properties change with temperature
- A linear function was fit to approximate thermal diffusivity
- A new thermal diffusivity value, α_{Layer}, is based on the average temperature in the layer before it, $\mathrm{T}_{\mathrm{Layer}}$

T [°C]	k [W·m^{-1}·°C^{-1}]	C_p [J·kg^{-1}·°C^{-1}]	Calculated α [m^2·s^{-1}]
20	6.6	565	2.64
93	7.3	565	2.92
205	9.1	574	3.58
250	9.7	586	3.74
315	10.6	603	3.97
425	12.6	649	4.38
500	13.9	682	4.60

$$\alpha_{\mathrm{Layer}} = 0.0042 \times \mathrm{T}_{\mathrm{Layer}} + 2.612$$

$$\mathbf{T}_c = \boldsymbol{\Phi} e^{-\alpha \mathrm{g} \boldsymbol{\Lambda} t_b} \boldsymbol{\Phi}' \mathrm{T}_0$$

Transient Material Properties

Goldak's Double Ellipsoid Heat Source

- The laser penetrates further into the part than just one layer
- Blocks below the meltpool must also be given an elevated temperature
- Layers below the deposition layer are called sublayers

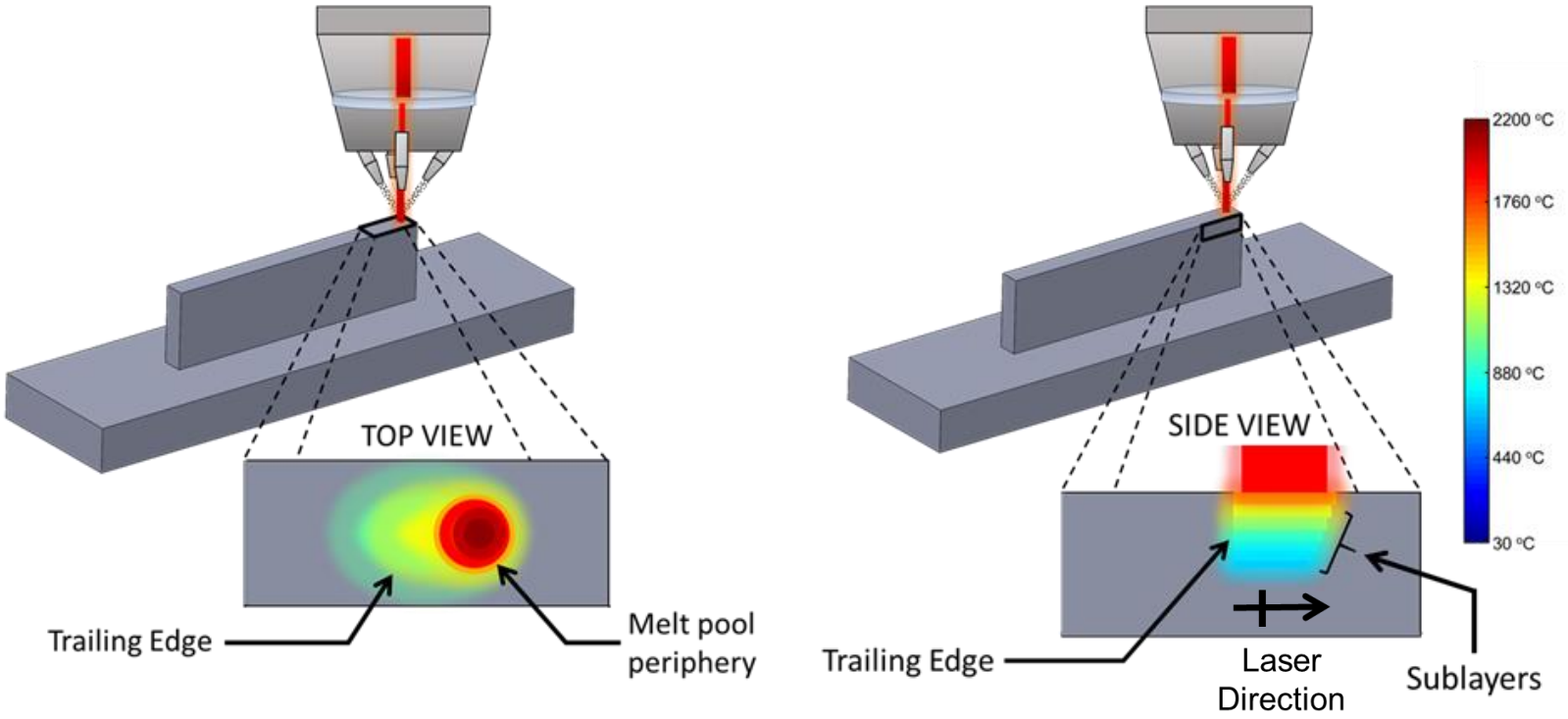

Laser Penetration

Goldak's Double Ellipsoid Heat Source

Goldak's model is taken from weld modeling and applied to laser-based processes.

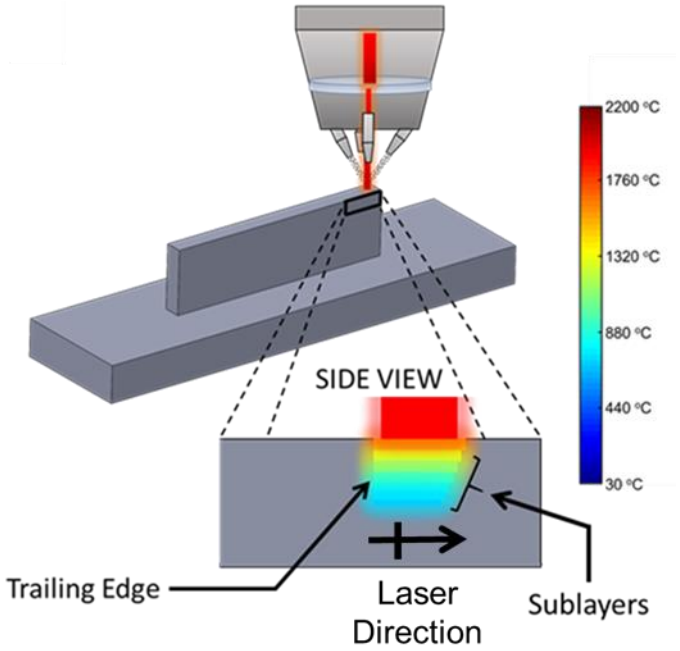

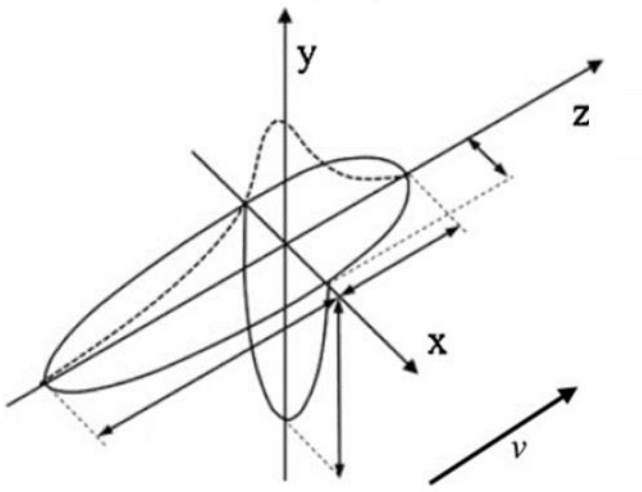

$$T_0(x, y, z, t) = C \times P \times \frac{1}{2\pi K\sqrt{x^2 + y^2 + z^2}} \times \exp\left[-\frac{v}{2\kappa} \times \left(x + \sqrt{x^2 + y^2 + z^2}\right)\right]$$

Moving Heat Source Model

Goldak's Double Ellipsoid Heat Source

- The unitless scaling factor, C, was used to set an upper limit on the temperature profile
- C is dependent on the meltpool temperature

$$T_0(x,y,z,t) = C \times P \times \frac{1}{2\pi K\sqrt{x^2+y^2+z^2}} \times \exp\left[-\frac{v}{2\kappa} \times \left(x+\sqrt{x^2+y^2+z^2}\right)\right]$$

Variable	Units	Value
C	Dimensionless	0.125 to 0.191
Laser Power (P)	[W]	415
Laser Velocity (v)	$[m \cdot s^{-1}]$	8.5×10^{-3}
Thermal Conductivity (K)	$[W \cdot m^{-1}K^{-1}]$	6.8
Thermal Diffusivity (κ)	$[m^2 \cdot s^{-1}]$	2.7228×10^{-6}

Scaling Factor: Justification

Meltpool Temperature (Literature)

The best way to validate is through experimentation, but some inconsistencies remain.

Geometry	Laser Power (P) [W]	Scan Speed [$mm \cdot s^{-1}$]	Method	Meltpool Temperature (T_0) [°C]
Thin Wall	300	12.7	Pyrometer	~1850
Thin Wall	290	12.7	Pyrometer	1900-2000
L-shaped Thin Wall	450	10.6	IR Camera	2485 ± 161
Cylinders	350	16.9	Pyrometer	2100 – 2500
Rectangular Thin Wall	300	2.0	Quiet Element Technique	2447
Cube	800	10.0	In-house Code (GAMMA)	2500
Thin Wall	425	8.5	Inactive Element Technique	1800 - 2000
My Values:	415	8.5		

Three meltpool temperatures selected in this work to represent the range of values observed: 1900 °C, 2200 °C, and 2450 °C.

Goldak's Double Ellipsoid Heat Source

- Starting point: Liquidus temperature (1630 °C) is reached at the periphery of the meltpool
- Center of the meltpool is hotter since it receives highest laser intensity and is surrounded by molten Ti-6Al-4V

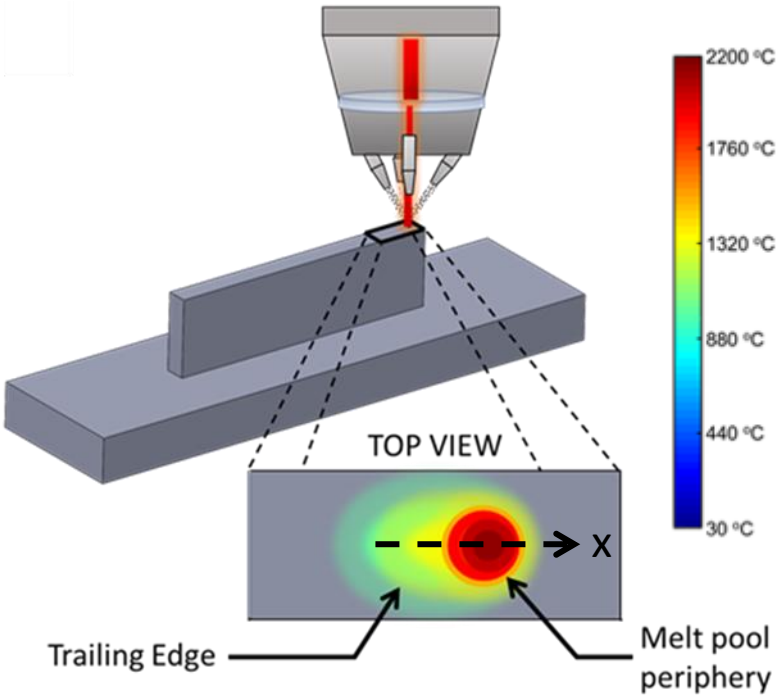

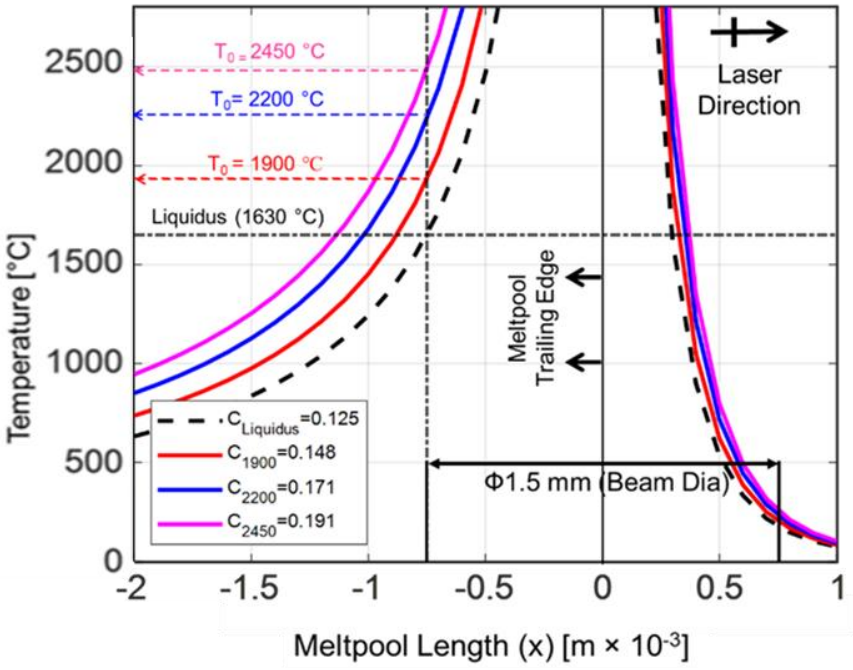

Scaling Factor: Profiles

Goldak's Double Ellipsoid Heat Source

Once the laser profile is consistent with reality, temperatures are found with respect to depth.

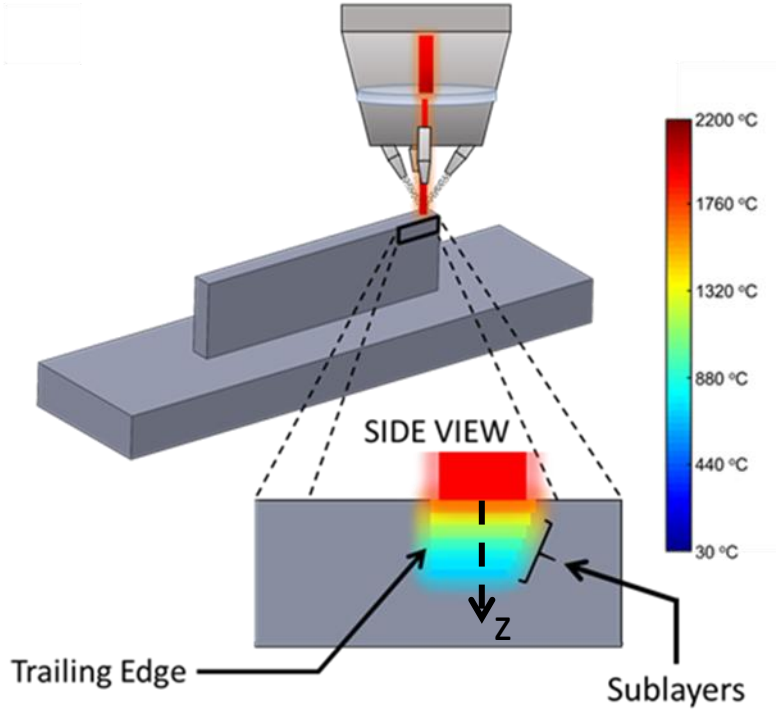

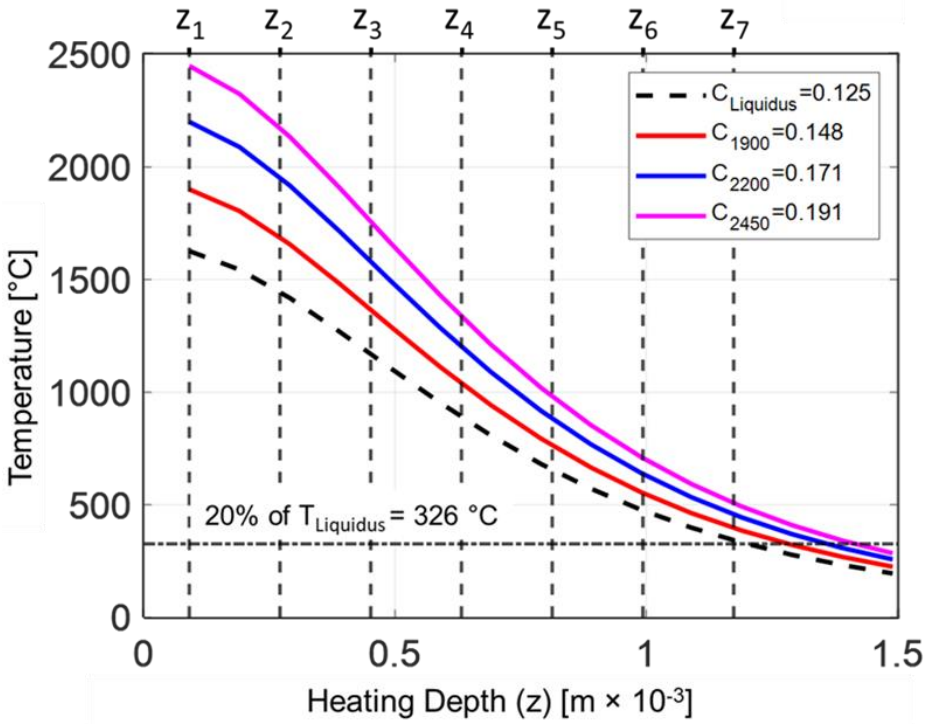

Scaling Factor: Depths

Goldak's Double Ellipsoid Heat Source

The implementation of Goldak's model is distilled into three steps.

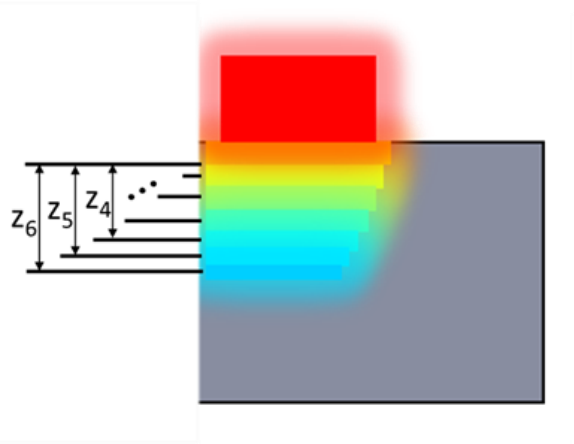

Step 1

- Set reference point
- Determine distance to the center of each sublayer

Implementing Goldak

Outline

- Context
- Methodology
- Results
  - Definitions
  - Case A Results
  - Case B Results
  - Case C Results
  - Summary
- Conclusions

Definitions

- Mean Absolute Percentage Error (MAPE)
- Root Mean Square Error (RMSE)
- Each simulation is repeated three times, and the uncertainty is quantified in terms of the standard deviation of error

$$MAPE = \frac{100\%}{n} \times \sum_{i=1}^{n} \left| \frac{T_i - \hat{T}_i}{T_i} \right|$$

$$RMSE = \sqrt{\sum_{i=1}^{n} \frac{\left(T_i - \hat{T}_i\right)^2}{n}}$$

Variable	Definition
n	Number of data points
i	Current instant of time
T_i	Measured temperature
$\hat{T}_i$	Simulated temperature

Case A Results

Due to the programmed 20-second dwell time, this case results in the lowest peak temperature (200 °C).

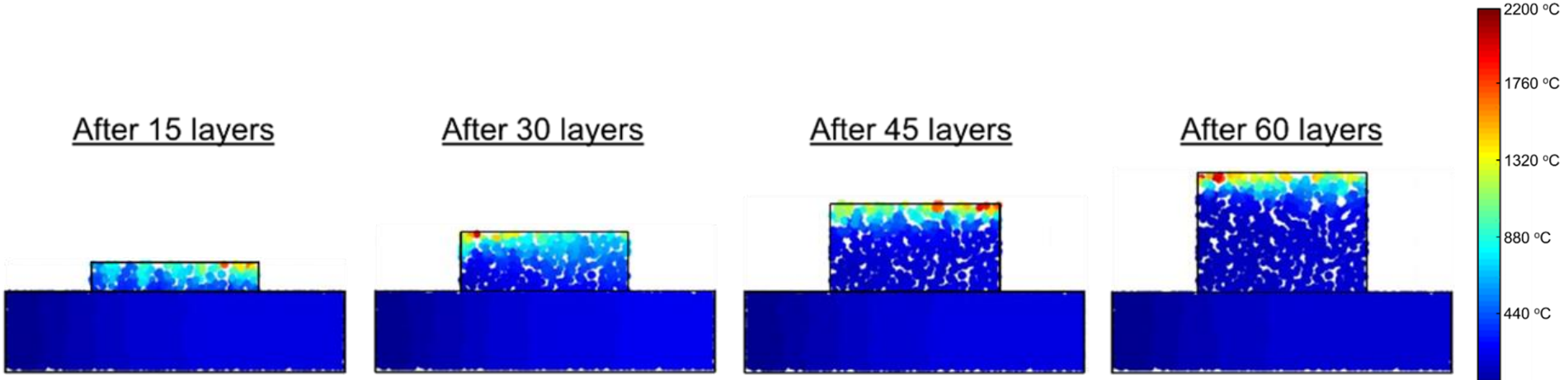

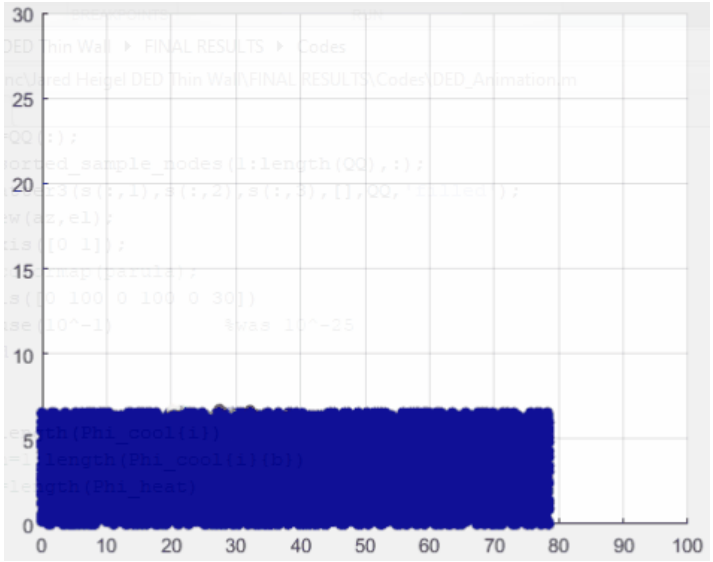

Case A Results

Prediction accuracy improves with increasing meltpool temperature.

1900 °C

0.4709 nodes/mm^3

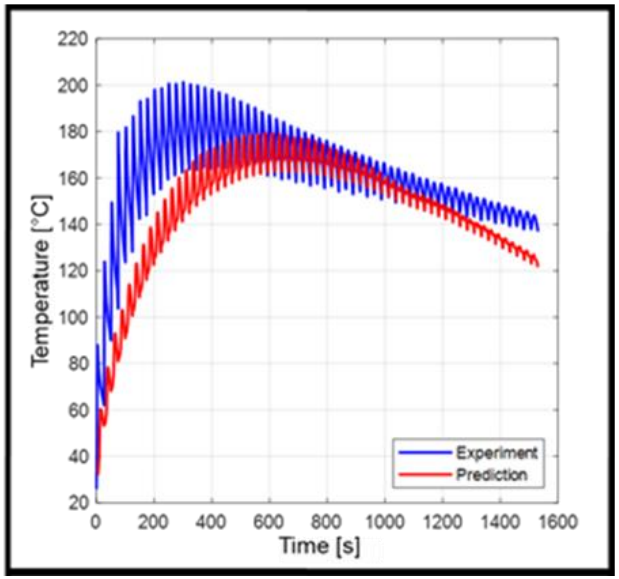

Case A Results

Prediction accuracy improves with increasing node density.

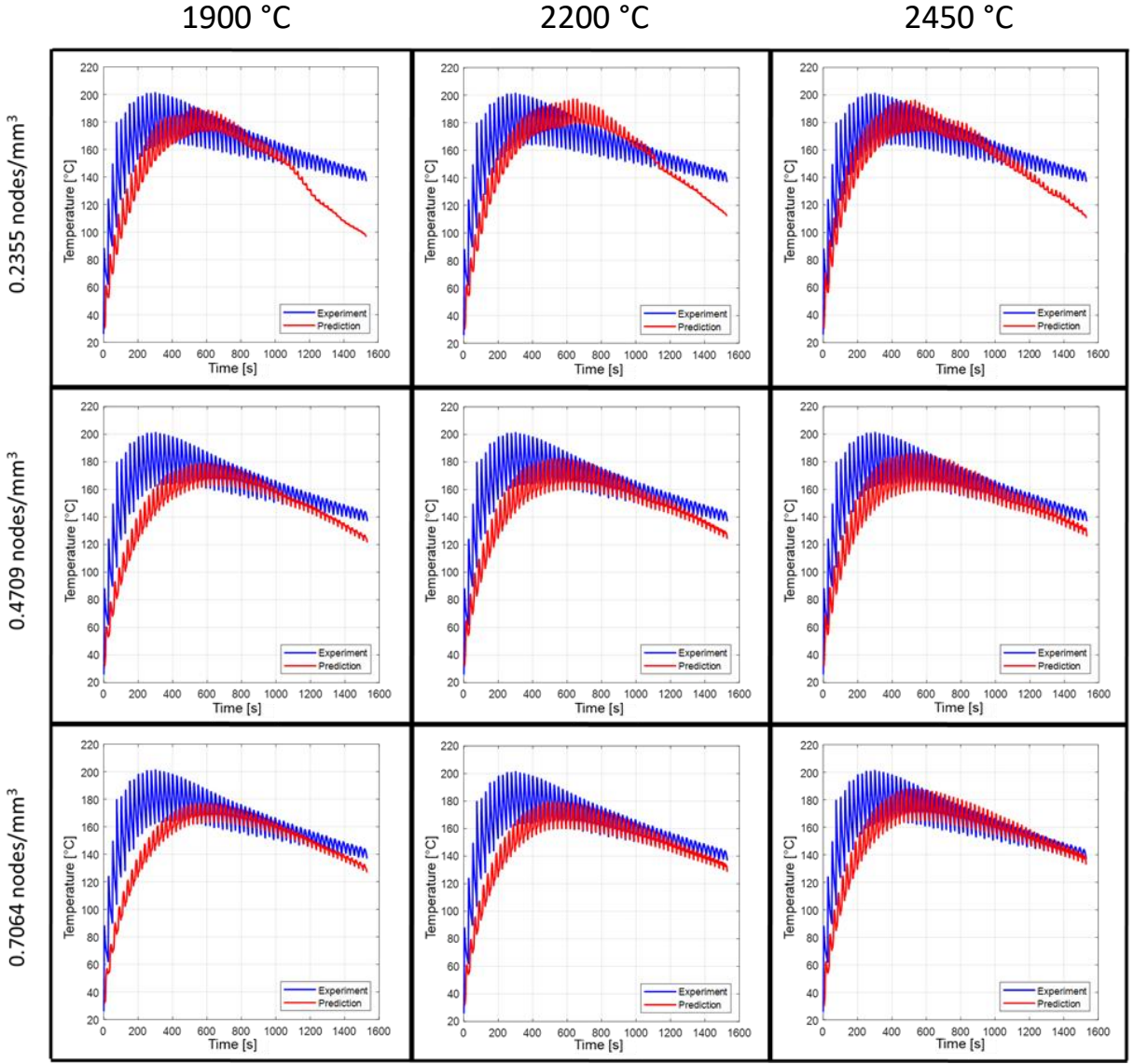

Case A Results

- For the simulation using one node with T_0 = 2200 °C, the MAPE is found to be 10.75%, and RMSE is 23 °C
- Can compute in 9 minutes on a desktop computer
- **Build time:** 25.6 minutes

Node Density [nodes·mm^{-3}]	Computation Time [min]	T_0 = 1900 °C		T_0 = 2200 °C		T_0 = 2450 °C	
		MAPE [%]	RMSE [°C]	MAPE [%]	RMSE [°C]	MAPE [%]	RMSE [°C]
0.2355 (1 node)	9	13.1 (1.4)	25.9 (1.6)	10.8 (2.0)	23.2 (2.8)	10.1 (4.5)	21.5 (6.9)
0.4709 (2 nodes)	82	9.8 (0.6)	22.8 (1.0)	7.7 (1.3)	18.8 (2.1)	7.6 (2.3)	17.7 (3.8)
0.7064 (3 nodes)	194	8.0 (1.6)	20.7 (1.7)	6.6 (1.1)	18.4 (1.4)	6.0 (2.6)	16.5 (2.9)

Case B Results

Without the dwell time, this case results in the highest peak temperature (500 °C).

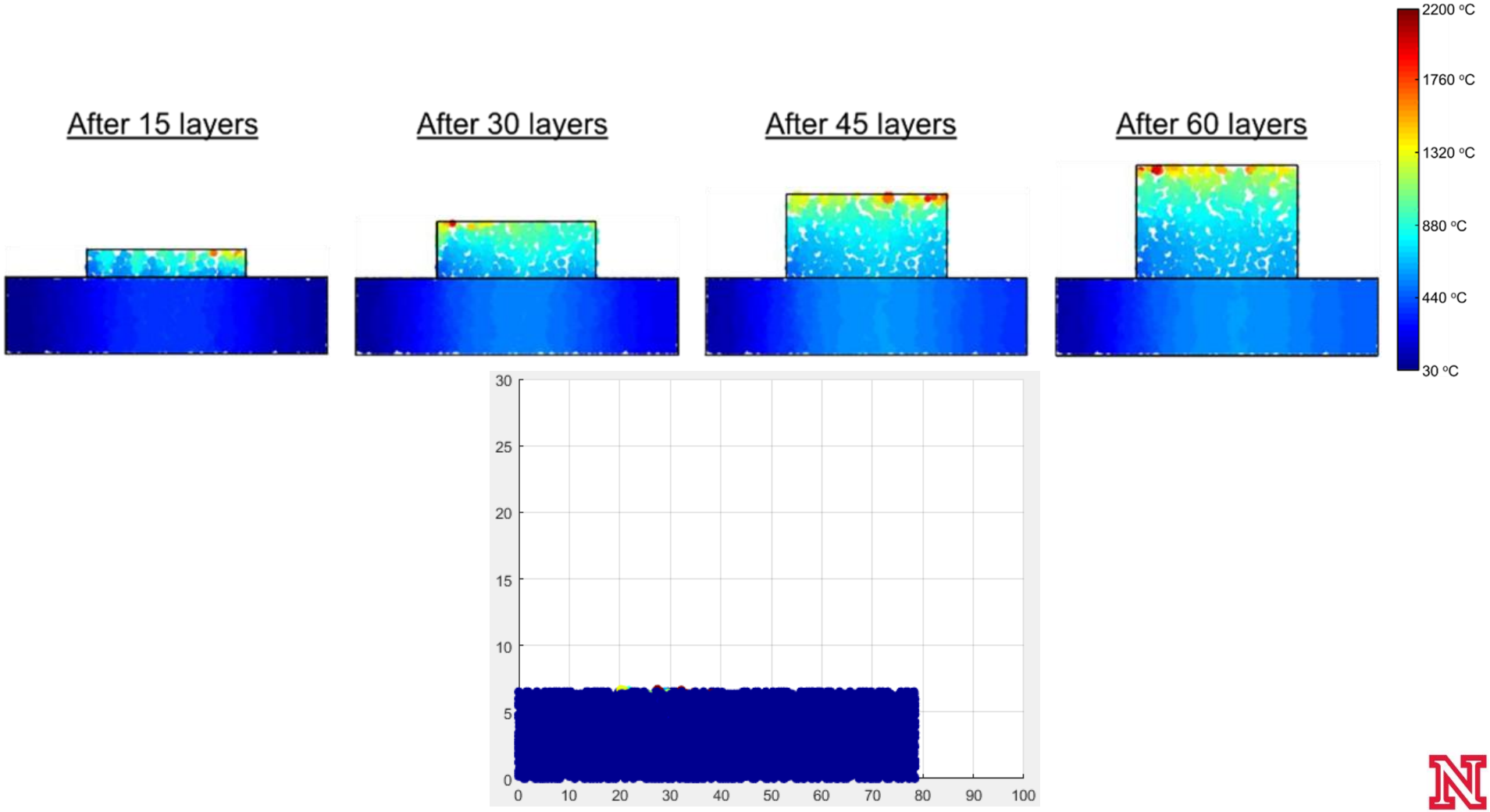

Case B Results

Prediction begins to exceed experiment when the same geometry is deposited without a dwell time.

1900 °C

0.4709 nodes/mm³

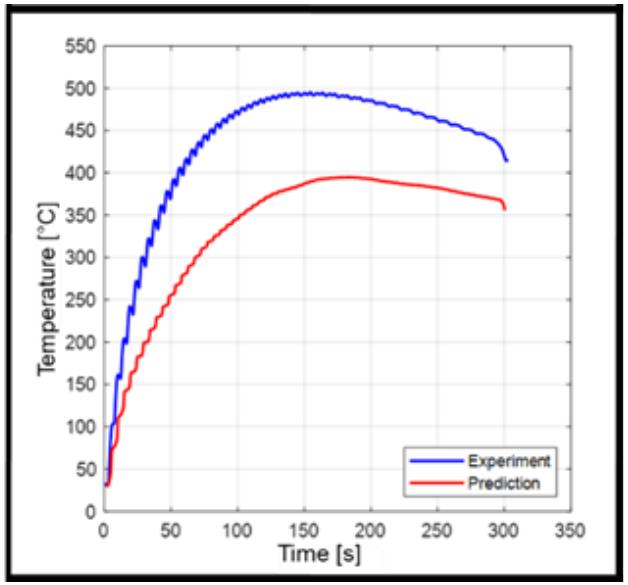

Case B Results

Major process physics are still being captured.

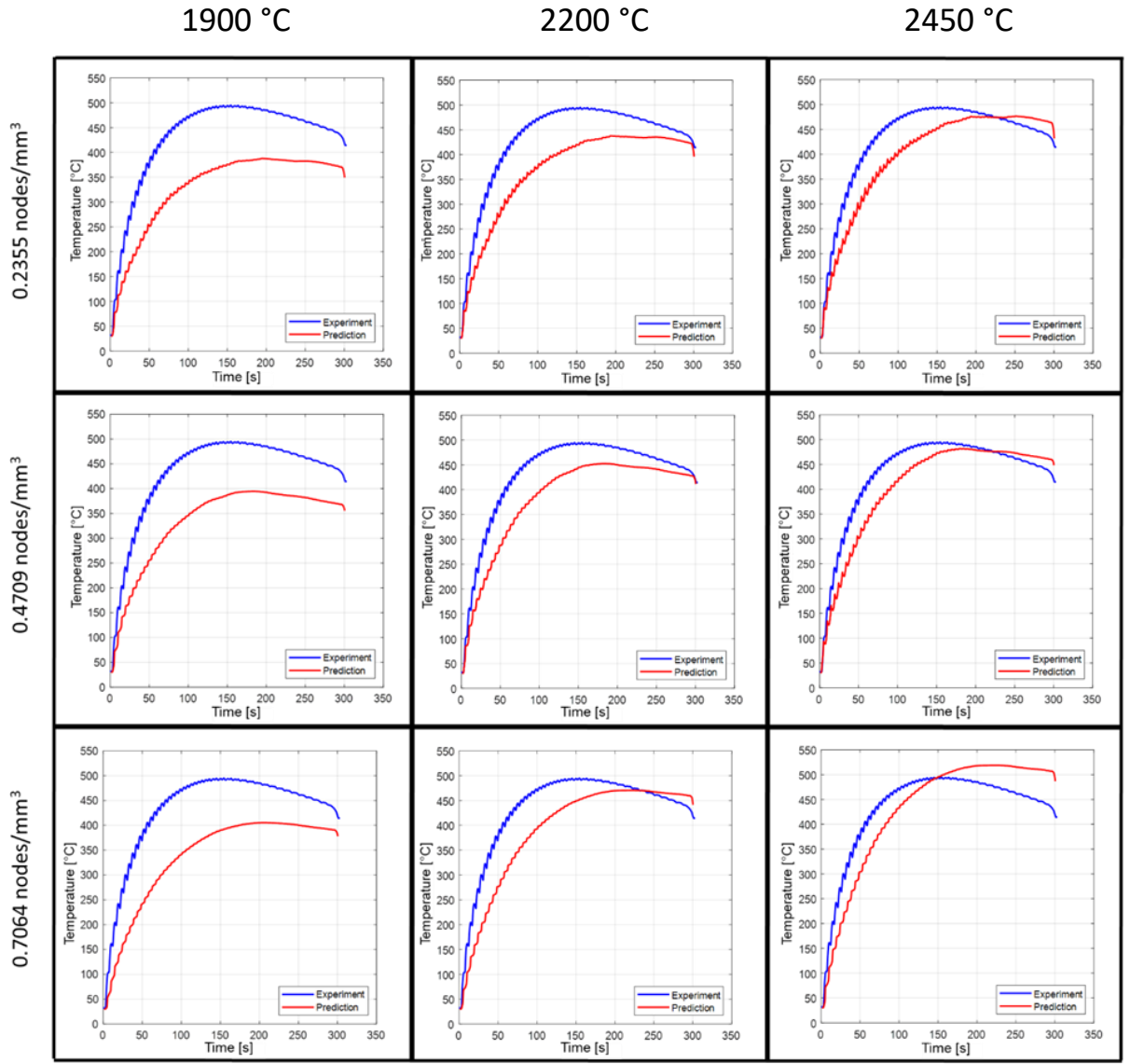

Case B Results

- For the simulation using one node with T_0 = 2200 °C, the MAPE is found to be 17%, and RMSE is 75 °C
- Can compute in 9 minutes on a desktop computer
- **Build time:** 5.2 minutes

Node Density [nodes·mm^{-3}]	Computation Time [min]	T_0 = 1900 °C		T_0 = 2200 °C		T_0 = 2450 °C	
		MAPE [%]	RMSE [°C]	MAPE [%]	RMSE [°C]	MAPE [%]	RMSE [°C]
0.2355 (1 node)	9	26.5 (2.6)	114.4 (11.5)	17.3 (1.6)	75.0 (5.3)	10.5 (2.8)	48.5 (11.6)
0.4709 (2 nodes)	82	24.5 (1.9)	105.2 (8.2)	12.7 (0.5)	59.5 (2.4)	10.5 (0.9)	49.5 (3.6)
0.7064 (3 nodes)	194	22.6 (0.5)	98.0 (1.6)	12.5 (0.9)	57.8 (3.8)	12.4 (0.5)	53.3 (3.1)

Case C Results

With the increased wall height and no dwell time, this case reaches a peak temperature of 300 °C.

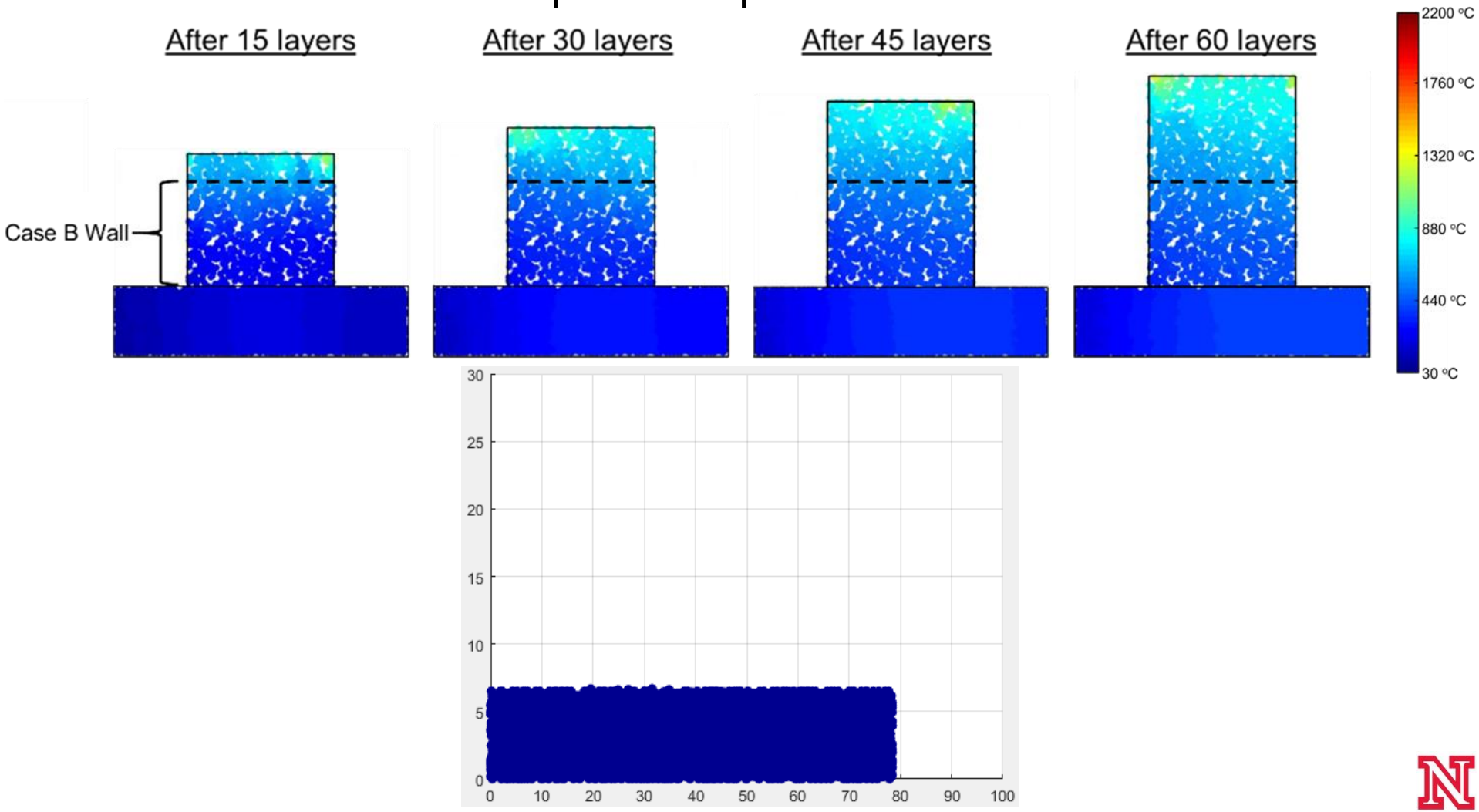

Case C Results

Prediction is not as accurate when given a new part geometry.

1900 °C

0.4709 nodes/mm³

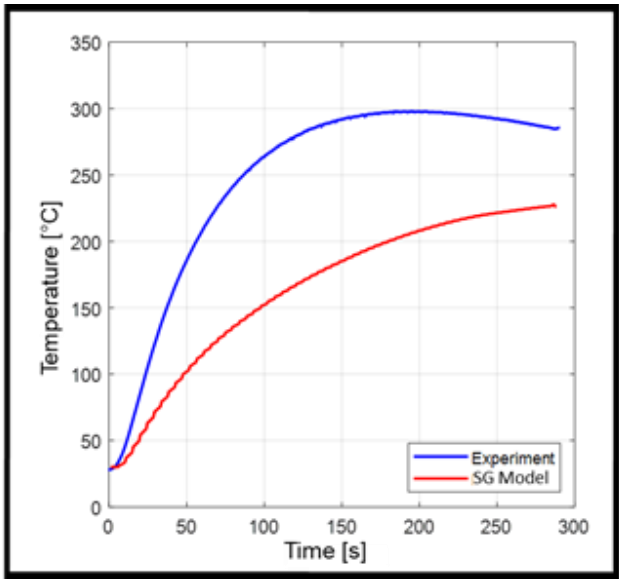

Case C Results

Acceptable but dominant heat transfer mechanism has changed.

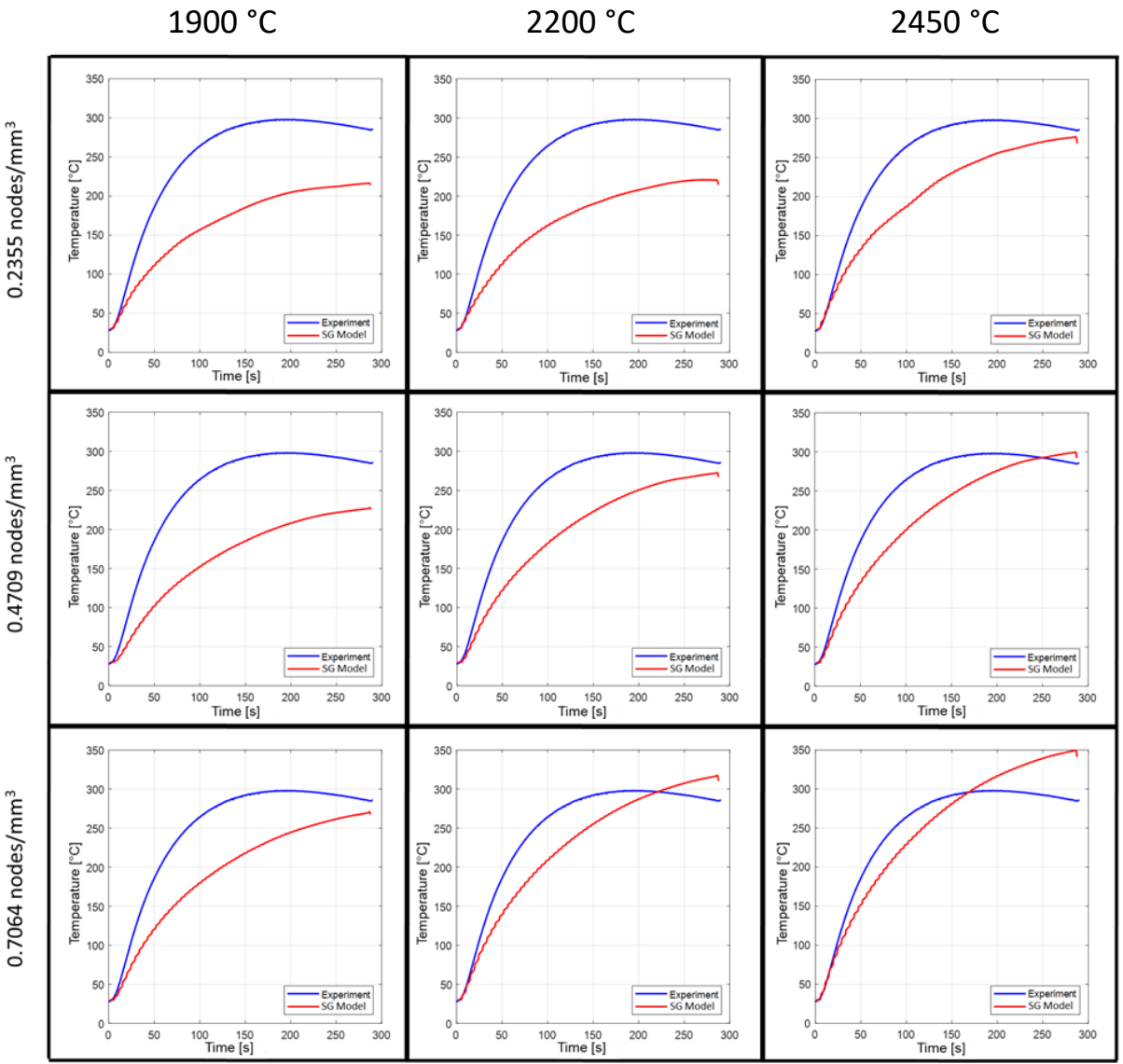

Case C Results

- For the simulation using one node with T_0 = 2200 °C, the MAPE is found to be 28%, and RMSE is 78 °C
- Can compute in 21 minutes on a desktop computer
- **Build time:** 10.1 minutes

Node Density [nodes·mm^{-3}]	Computation Time [min]	T_0 = 1900 °C		T_0 = 2200 °C		T_0 = 2450 °C	
		MAPE [%]	RMSE [°C]	MAPE [%]	RMSE [°C]	MAPE [%]	RMSE [°C]
0.2355 (1 node)	21	31.6 (4.0)	84.9 (10.7)	28.2 (2.0)	78.6 (5.5)	16.7 (0.5)	45.7 (1.6)
0.4709 (2 nodes)	188	32.0 (1.1)	84.0 (2.7)	19.7 (0.2)	51.7 (0.9)	12.5 (1.2)	35.0 (5.2)
0.7064 (3 nodes)	650	21.8 (1.1)	55.3 (3.4)	10.0 (0.7)	26.1 (3.3)	9.3 (3.4)	28.0 (14.6)

Summary

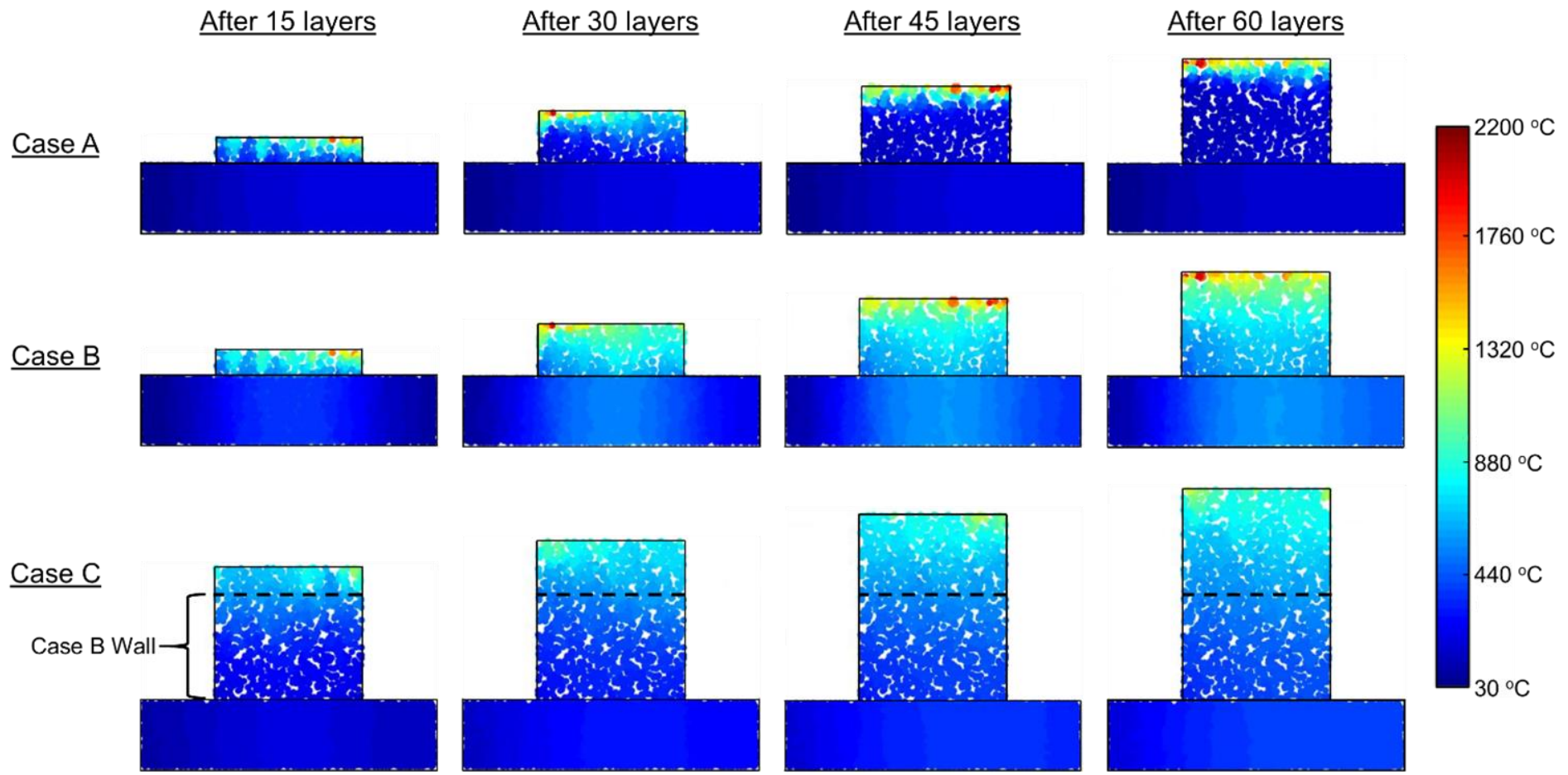

Simulation Snapshots

Outline

- Context
- Methodology
- Results
- Conclusions
  - Takeaways
  - Future Work

Takeaways

The graph-theoretic approach can provide valid thermal predictions for the DED process at a relatively low computational expense.

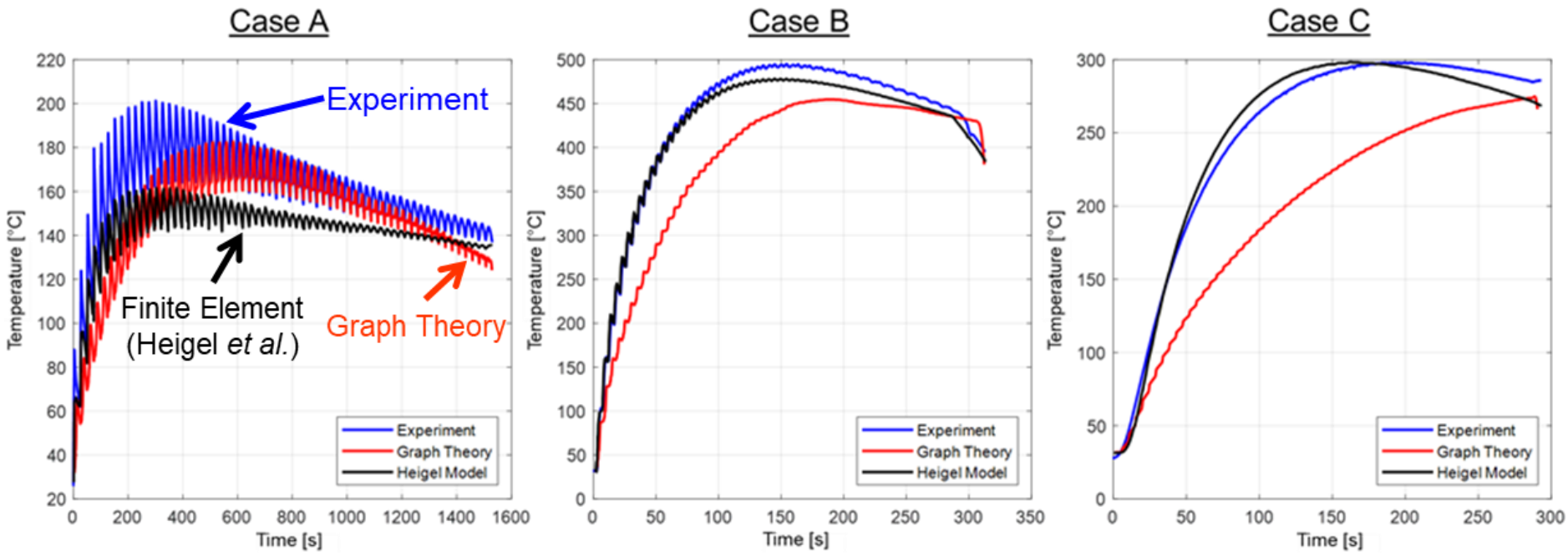

Takeaways

- Computation time reported for Heigel's model is for the part's half-symmetry
- A calculated error of approximately 20% was attainable for each case while simulating the entire part

Data	Case A		Case B		Case C	
	Time [min]	MAPE [%]	Time [min]	MAPE [%]	Time [min]	MAPE [%]
Finite Element (Heigel Model)	136	10.4	136	2.4	No Report	4.1
Graph Theory	82	7.59	82	11.94	188	19.79
Build Time	25.6 minutes		5.2 minutes		10.1 minutes	

Future Work

1. Obtain meltpool temperature directly from the experiment
    - This would allow for a better calibration and corresponding prediction

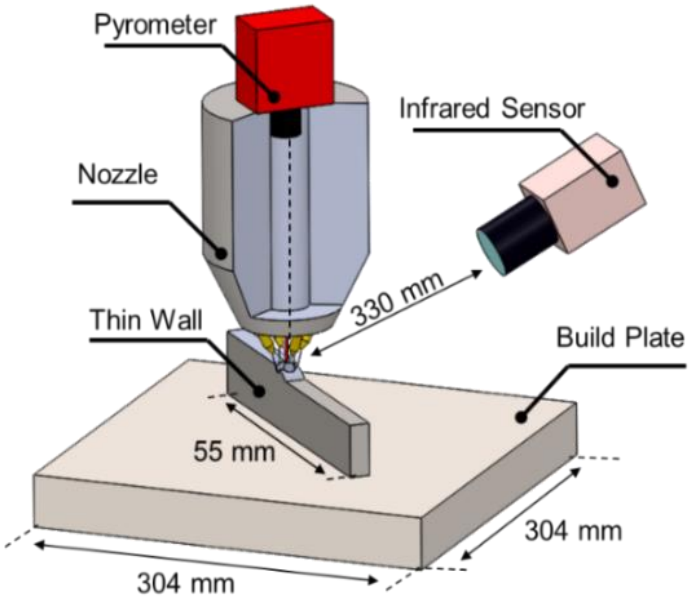

2. Resolve disproportionate boundary node quantities
    - Extra heat losses associated with convection and radiation are applied to the boundary nodes
    - 15% more heat loss in the lowest node density case

A.C. Gaikwad, R. Yavari, M. Montazeri, K. Cole, L. Bian, P. Rao. Toward the Digital Twin in Metal Additive Manufacturing – Integrating Thermal Simulations, Sensing, and Analytics to Detect Process Faults, IISE Transactions (Accepted, in-press, available online) doi: 10.1080/24725854.2019.1701753

Future Work

3. Implement more rigorous radiative heat loss approximation
   - A new radiation approximation appeared to improve the prediction accuracy for only Case B

Case B

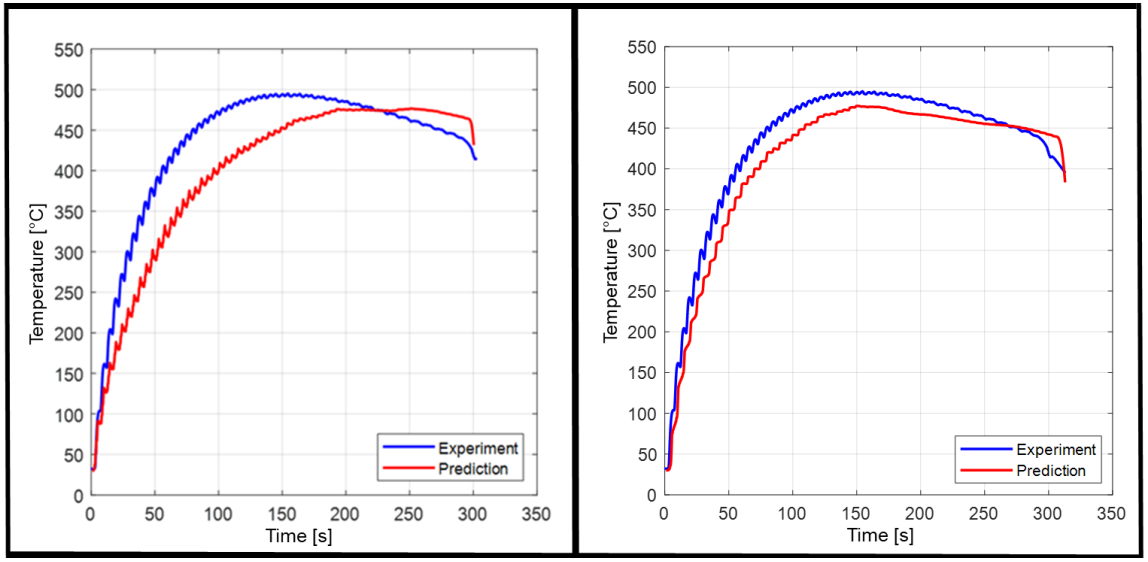

4. Develop method for changing node density in the substrate
   - Lower node count will reduce computation time

Obtaining Eigenvectors (ϕ) and Eigenvalues (Λ)

Adjacency matrix $A \stackrel{\text{def}}{=} [a_{ij}]$

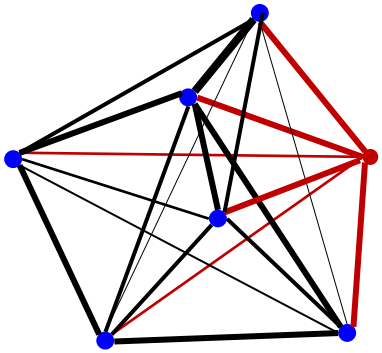

k

$$d_k = \sum_{j=1}^{j=M} w_{kj}$$

Degree matrix

$$\mathcal{D} \stackrel{\text{def}}{=} \begin{bmatrix} d_1 & 0 & 0 \\ 0 & d_k & 0 \\ 0 & 0 & d_M \end{bmatrix}$$

Sum each row of the Similarity matrix, and put it on the diagonal

Laplacian matrix

$$\mathcal{L} \stackrel{\text{def}}{=} (\mathcal{D} - A)$$

$$\mathcal{L}\phi = \Lambda\phi$$

M. R. Yavari, K. Cole, and P. Rao, "Thermal Modeling in Metal Additive Manufacturing using Graph Theory," *ASME Transactions, Journal of Manufacturing Science and Engineering,* vol. 141, pp. 071007-27, July 2019.